JOURNAL OF GEOPHYSICAL RESEARCH, VOL. 113, A02304, doi:10.1029/2007JA012787, 2008

Experimental and coupled-channels investigation of the radiative properties of the N_2 $c_4' \, ^1\Sigma_u^+ - X \, ^1\Sigma_g^+$ band system

Xianming Liu,[1] Donald E. Shemansky,[1] Charles P. Malone,[2] Paul V. Johnson,[2] Joseph M. Ajello,[2] Isik Kanik,[2] Alan N. Heays,[3] Brenton R. Lewis,[3] Stephen T. Gibson,[3] and Glenn Stark[4]

Received 31 August 2007; revised 28 September 2007; accepted 6 November 2007; published 14 February 2008.

[1] The emission properties of the N_2 $c_4' \, ^1\Sigma_u^+ - X \, ^1\Sigma_g^+$ band system have been investigated in a joint experimental and coupled-channels theoretical study. Relative intensities of the $c_4' \, ^1\Sigma_u^+(0) - X \, ^1\Sigma_g^+(v_i)$ transitions, measured via electron-impact-induced emission spectroscopy, are combined with a coupled-channel Schrödinger equation (CSE) model of the N_2 molecule, enabling determination of the diabatic electronic transition moment for the $c_4' \, ^1\Sigma_u^+ - X \, ^1\Sigma_g^+$ system as a function of internuclear distance. The CSE rotational transition probabilities are further verified by comparison with a high-resolution experimental spectrum. Spontaneous transition probabilities of the $c_4' \, ^1\Sigma_u^+ - X \, ^1\Sigma_g^+$ band system, required for modeling atmospheric emission, can now be calculated reliably.

Citation: Liu, X., D. E. Shemansky, C. P. Malone, P. V. Johnson, J. M. Ajello, I. Kanik, A. N. Heays, B. R. Lewis, S. T. Gibson, and G. Stark (2008), Experimental and coupled-channels investigation of the radiative properties of the N_2 $c_4' \, ^1\Sigma_u^+ - X \, ^1\Sigma_g^+$ band system, *J. Geophys. Res.*, *113*, A02304, doi:10.1029/2007JA012787.

1. Introduction

[2] Molecular nitrogen is the major component of the atmospheres of the Earth, Titan and Triton. The N_2 airglow emissions from the atmospheres of the Earth [*Morrison et al.*, 1990; *Meier*, 1991; *Feldman et al.*, 2001; *Strickland et al.*, 2004a, 2004b; *Bishop et al.*, 2005, 2007] and planetary satellites [*Broadfoot et al.*, 1989; *Liu et al.*, 2005b] have been observed extensively. The interpretation and modeling of atmospheric excitation of N_2 by photons and photoelectrons requires accurate and comprehensive information on line positions, oscillator strengths, transition probabilities and predissociation rates.

[3] Nitrogen is the fifth most abundant element in the universe. Its presence in the interstellar medium is thought to be mostly in molecular form, although this belief has been questioned recently by *Maret et al.* [2006]. The abundance of N_2 in the interstellar medium is poorly known due to the lack of allowed pure rotational and vibrational transitions in this homonuclear molecule. It is only recently that an electronic transition of N_2 has been detected in the interstellar medium, namely the strong $c_4' \, ^1\Sigma_u^+(0) - X \, ^1\Sigma_g^+(0)$ band [*Knauth et al.*, 2004]. In comets, the inferred N_2 abundance is very low and the nitrogen elemental abundance is smaller than the solar value [*Cochran et al.*, 2000; *Iro et al.*, 2003].

[4] Strong dipole-allowed transitions of N_2 in the extreme ultraviolet (EUV) region arise from the ground $X \, ^1\Sigma_g^+$ state to singlet ungerade excited states, which consist of two valence states, $b' \, ^1\Sigma_u^+$ and $b \, ^1\Pi_u$, and three Rydberg series, $np\sigma$, $np\pi$ and $ns\sigma$. The $np\sigma$ and $np\pi$ series, both converging to the $X \, ^2\Sigma_g^+$ state of N_2^+, are usually labeled as $c_{n+1}' \, ^1\Sigma_u^+$ and $c_n \, ^1\Pi_u$, while the $ns\sigma$ series, converging to the N_2^+ $A \, ^2\Pi_u$ state, is usually designated as $o_n \, ^1\Pi_u$. The spectrum of the singlet *ungerade* states displays many irregularities in both ro-vibronic energy levels and intensity distribution. *Stahel et al.* [1983] showed that homogeneous interactions within the $^1\Sigma_u^+$ and $^1\Pi_u$ manifolds, primarily of the Rydberg-valence type, are the cause of most of the irregularities. *Spelsberg and Meyer* [2001] carried out *ab initio* calculations on the three lowest members of the $^1\Sigma_u^+$ and $^1\Pi_u$ manifolds by introducing coupling that varies with internuclear distance, and achieved much better agreement with experimental results. *Carroll and Yoshino* [1972] analyzed the interaction between the $c_{n+1}' \, ^1\Sigma_u^+$ and $c_n \, ^1\Pi_u$ series with **L**-uncoupling theory. *Helm et al.* [1993], *Edwards et al.* [1995], *Ubachs et al.* [2001], and *Sprengers et al.* [2003] extended the work of *Stahel et al.* [1983] by introducing the Rydberg *p*-complex $^1\Sigma_u^+ \sim {}^1\Pi_u$ heterogeneous interaction. More recently, *Lewis et al.* [2005a, 2005b] and *Haverd et al.* [2005] considered additional interactions between the singlet and triplet Π_u^f states within a coupled-channel Schrödinger equation (CSE) model which has succeeded in

[1]Planetary and Space Science Division, Space Environment Technologies, Pasadena, California, USA.
[2]Jet Propulsion Laboratory, California Institute of Technology, Pasadena, California, USA.
[3]Research School of Physical Sciences and Engineering, The Australian National University, Canberra, Australian Capital Territory, Australia.
[4]Department of Physics, Wellesley College, Wellesley, Massachusetts, USA.

0148-0227/08/2007JA012787$09.00

explaining quantitatively the N_2 predissociation mechanism for the first time.

[5] Transitions to the valence states, $b'\ ^1\Sigma_u^+$ and $b\ ^1\Pi_u$, and to the lowest members ($n = 3$) of the Rydberg series ($c'_4\ ^1\Sigma_u^+$, $c_3\ ^1\Pi_u$, and $o_3\ ^1\Pi_u$) carry the largest oscillator strengths in N_2 neutral transitions. They have been investigated extensively by many experimental techniques, including photoabsorption [*Carroll and Collins*, 1969; *Carroll et al.*, 1970; *Yoshino et al.*, 1975, 1979; *Yoshino and Tanaka* 1977; *Stark et al.*, 1992, 2000, 2005], low-pressure discharge emission [*Roncin et al.*, 1998, 1999], electron-energy-loss [*Geiger and Schröder*, 1969; *Trajmar et al.*, 1983; *Chan et al.*, 1993; *Khakoo et al.*, 2007] electron-impact-induced emission [*Ajello et al.*, 1989, 1998; *James et al.*, 1990; *Shemansky et al.*, 1995; *Liu et al.*, 2005a], synchrotron-radiation-induced fluorescence [*Gürtler et al.*, 1977; *Oertel et al.*, 1981; *Wu et al.*, 2007], and nonlinear laser techniques [*Kam et al.*, 1989; *Helm and Cosby*, 1989; *Helm et al.*, 1993; *Walter et al.*, 1993, 1994, 2000; *Levelt and Ubachs*, 1992; *Ubachs et al.*, 1989, 2000; *Sprengers et al.*, 2003, 2004a, 2005; *Sprengers and Ubachs*, 2006]. These investigations have shown that strong coupling among the singlet states results in major energy-level and intensity perturbations, and that significant predissociation occurs for many of the excited levels.

[6] The excitation of the N_2 Carroll-Yoshino (CY) $c'_4\ ^1\Sigma_u^+(0) - X\ ^1\Sigma_g^+$ system plays an important role in establishing the states of the nitrogen-rich planetary atmospheres. The N_2 $c'_4\ ^1\Sigma_u^+(0) - X\ ^1\Sigma_g^+(0)$ band has the largest electron excitation and emission cross sections in the EUV region [*Ajello et al.*, 1989]. The excitation of this system is the major absorber of energy in N_2, and the dispersal of this energy plays a critical role in establishing the state of the atmosphere. Predissociation in the CY system radicalizes the state of nitrogen in the atmosphere. Multiple scattering in the (0,0) band drastically reduces the photon flux escaping from the excited volume, leaving most of the energy deposited locally. For this reason, the (0,0) band is observed to be weak in all of the nitrogen dominated atmospheres, including Titan [*Strobel and Shemansky*, 1982; *Hall et al.*, 1992; *Liu et al.*, 2005b], Triton [*Broadfoot et al.*, 1989], and Earth [*Zipf and McLaughlin*, 1978; *Morrison et al.*, 1990; *Stevens et al.*, 1994; *Feldman et al.*, 2001; *Bishop et al.*, 2005, 2007]. In contrast, the brightness of the N_2^+ $B\ ^2\Sigma_u^+ - X\ ^2\Sigma_g^+$ band system, having $\sim$3 times larger 100 eV excitation cross section from the N_2 $X\ ^1\Sigma_g^+(0)$ level, is frequently observed in the kilo-Rayleigh range [*Romick et al.*, 1999], and is used as an emission standard. It is clear that non-radiative losses of the excited singlet *ungerade* states, via dissociation, predissociation, and multiple scattering, dominate in excited N_2 atmospheres. Thus interpretation of airglow observations depends critically on both the radiative and non-radiative properties of the $c'_4\ ^1\Sigma_u^+(0) - X\ ^1\Sigma_g^+(v_i)$ transitions.

[7] Radiative parameters for the singlet *ungerade* states of N_2, except for those involving the $v_i = 0$ level of the $X\ ^1\Sigma_g^+$ state, have not been established definitively. Most experimental measurements have been confined to absorption cross sections for the discrete transitions from the $X\ ^1\Sigma_g^+(0)$ state [*Watanabe and Marmo*, 1956; *Lawrence et al.*, 1968; *Carter*, 1972; *Gürtler et al.*, 1977; *Chan et al.*, 1993]. The high-resolution photoabsorption measurements of *Stark et al.* [1992, 2000, 2005] have established accurate line oscillator strengths for many vibrational bands of the $b'\ ^1\Sigma_u^+$, $b\ ^1\Pi_u$, $c'_4\ ^1\Sigma_u^+$, $c_3\ ^1\Pi_u$ and $o_3\ ^1\Pi_u - X\ ^1\Sigma_g^+(0)$ transitions. Because of the strong ro-vibronic coupling among the *ungerade* levels, the experimental oscillator strengths show strong dependences on the rotational quantum number, and the *P*-, *Q*-, and *R*-branch ratios for many bands deviate significantly from Hönl-London-factor-based predictions. Radiative parameters, such as transition probabilities, between the singlet ungerade levels and vibrationally excited levels of the $X\ ^1\Sigma_g^+$ state, however, are generally unavailable. Although the photoabsorption of vibrationally excited N_2 prepared in a discharge has been reported [*Verma and Jois*, 1984], no accurate intensity measurements for transitions involving the $v_i > 0$ levels of the $X\ ^1\Sigma_g^+$ state are available, presumably because of difficulty in quantifying the relative populations of the vibrationally excited states. While the discharge-emission work of *Roncin et al.* [1998, 1999] is extremely valuable for the determination of accurate line positions and energy term values, it yields very little information on emission properties, primarily due to the optically thick nature of the experiments. While emission cross sections from some v_j levels of the ungerade states have been measured in low-resolution electron-impact experiments [*Ajello et al.*, 1989; *James et al.*, 1990], these measurements suffered from spectral blending and uncertainties in the calibration of spectrometer sensitivity, and are thus not sufficiently reliable.

[8] Using semi-empirical techniques, *Stahel et al.* [1983] obtained vertical transition moments for excitation of the $b'\ ^1\Sigma_u^+$, $c'_4\ ^1\Sigma_u^+$, $c_5'\ ^1\Sigma_u^+$, $b\ ^1\Pi_u$, $c_3\ ^1\Pi_u$ and $o_3\ ^1\Pi_u$ states from the $X\ ^1\Sigma_g^+(0)$ ground-state level. Ab initio transition moments for these band systems have been calculated recently by *Spelsberg and Meyer* [2001], over a wide range of internuclear distance *R*. For the most part, the magnitudes of the ab initio moments for vertical transitions agree fairly well with those obtained by *Stahel et al.* [1983], but there is a serious discrepancy in the case of the $o_3\ ^1\Pi_u - X\ ^1\Sigma_g^+$ transition, including the sense of its interference effect with the $b\ ^1\Pi_u - X\ ^1\Sigma_g^+$ transition [*Lewis et al.*, 2005a]. Furthermore, *Sprengers et al.* [2004a] and *Haverd et al.* [2005] noted that the *Spelsberg and Meyer* [2001] transition moments yield greater oscillator strengths for transitions to the $b\ ^1\Pi_u$, $c_3\ ^1\Pi_u$ and $o_3\ ^1\Pi_u$ states than the corresponding experimental values of *Stark et al.* [1992, 2005]. On the basis of the experimental photoabsorption oscillator strengths of *Stark et al.* [2005], *Haverd et al.* [2005] constructed a set of linearly *R*-dependent diabatic transition moments for the $b\ ^1\Pi_u - X\ ^1\Sigma_g^+$, $c_3\ ^1\Pi_u - X\ ^1\Sigma_g^+$, and $o_3\ ^1\Pi_u - X\ ^1\Sigma_g^+$ band systems of N_2, valid for 1.05 Å $< R <$ 1.20 Å.

[9] The present paper reports a combined experimental and theoretical investigation of the $c'_4\ ^1\Sigma_u^+ - X\ ^1\Sigma_g^+$ band system. The experiments focus specifically on the measurement of relative intensities for the $c'_4\ ^1\Sigma_u^+(0) - X\ ^1\Sigma_g^+(v_i)$ bands, using electron-impact-induced emission spectroscopy. The theoretical study, guided by the experimental relative intensities, together with the high-resolution photoabsorption oscillator strengths of *Stark et al.* [1992, 2000, 2005], employs a CSE model of electronic-state interactions in N_2 to determine the diabatic transition moment and spontaneous transition probabilities for the

$c'_4\ ^1\Sigma_u^+(0) - X\ ^1\Sigma_g^+$ system. The reliability of the calculated line transition probabilities is verified in detail by comparison with our experimental high-resolution spectra of the $c'_4\ ^1\Sigma_u^+(0) - X\ ^1\Sigma_g^+(v_i = 0-2)$ bands.

[10] The present experiments represent a continuation of, and, more importantly, a refinement of those reported by some of us [*Ajello et al.*, 1989, 1998; *James et al.*, 1990; *Shemansky et al.*, 1995; *Liu et al.*, 2005a, 2005b] over the last 18 years. The high-resolution measurements enable detailed examination and removal of the contributions of some overlapping spectral transitions. The more precise instrumental spectral sensitivity calibration using the e+H_2 standard [*Liu et al.*, 1995, 2002, 2003; *Abgrall et al.*, 1997; *Jonin et al.*, 2000], developed in the past 12 years, results in much more accurate relative intensity measurements. The improvement in the sensitivity of the system enables relative intensities to be measured under optically thin conditions. The results of the present investigation are also timely, as the recent theoretical investigations of *Lewis et al.* [2005a] and *Haverd et al.* [2005], using the CSE method, have successfully reproduced experimental oscillator-strength values and predissociation rates for various rotational levels of the low v_j levels of the $b\ ^1\Pi_u$, $c_3\ ^1\Pi_u$ and $o_3\ ^1\Pi_u$ states. The present extension of the CSE model to include a consideration of the $^1\Sigma_u^+$ states, informed by the current experimental measurements, leads to a reliable determination of the diabatic $c'_4\ ^1\Sigma_u^+ - X\ ^1\Sigma_g^+$ electronic transition moment, thus enabling the extensive calculations of the N_2 radiative parameters that are needed for modeling data from Far Ultraviolet Spectroscopic Explorer (FUSE) observation of the Earth dayglow [*Feldman et al.*, 2001; *Bishop et al.*, 2005, 2007] and Cassini UVIS observations of Titan [*Liu et al.*, 2005b].

2. Experiment

[11] The major components of the experimental setup have been described in detail by *Liu et al.* [1995, 2005a], with the exception of the improvements described below. The system consists of a 3-m spectrometer (Acton VM-523-SG) and an electron collision chamber. Electrons generated by heating a thoriated tungsten filament are magnetically collimated by an axially symmetric magnetic field of ~100 G and accelerated to a kinetic energy of 20 or 100 eV. Horizontally accelerated electrons collide with either a vertical beam of N_2 gas formed by a capillary array (cross beam mode) or with a uniform swarm of N_2 gas (swarm mode). In the cross beam mode, the cylindrical interaction region is ~3 mm in length and ~2 mm in diameter. Optical emission from electron-impact-excited N_2 is dispersed by the spectrometer that is equipped with a 1200 grooves mm^{-1} grating. The spectrometer has an aperture ratio of *f*/28.8 and a field of view of 3.8 mm (horizontal) by 2.4 mm (vertical). The dispersed radiation is detected with a channel electron multiplier coated with CsI. A Faraday cup is utilized to monitor the beam current and to minimize the backscattered electrons. A calibrated ionization gauge is used to monitor the N_2 pressure in the collision chamber.

[12] Several improvements have been made since the work of *Liu et al.* [2005a]. In the previous work, a 1200 grooves mm^{-1} grating coated with Al+MgF_2 was used. In the present experiment, a custom-coated B_4C concave grating with 1200 grooves $mm^{-1)}$ is utilized. The new grating, 104 × 65 mm in size, was blazed at 1200 Å with an angle of 4°7′. It has an efficiency in first order of 38.2%, 38.6% and 37.6% at 920, 1025 and 1215 Å, respectively. In comparison with the previously used Al+MgF_2 coating, the B_4C coating increases the sensitivity by a factor of 4 to 1.6 in the 800 Å to 1150 Å region. Near 960 Å, where the $c'_4\ ^1\Sigma_u^+(0) - X\ ^1\Sigma_g^+(0)$ transition occurs, the estimated sensitivity enhancement is on the order of 2.5. The improvement in sensitivity allows the measurement to be made at significantly lower N_2 sample pressures than those of *Liu et al.* [2005a] and *Ajello et al.* [1989] (discussed below). Changes have also been made to the data acquisition system so that it simultaneously records spectral signal, Faraday cup current and sample pressure at each data point.

[13] Minimizing self-absorption of the N_2 emission is extremely important for accurate relative intensities. The large oscillator strength and blended rotational transitions of the $c'_4\ ^1\Sigma_u^+(0) - X\ ^1\Sigma_g^+(0)$ band require that the measurement be carried out at very low pressures. Several difficulties were encountered in the cross-beam measurement. First, the cross-beam configuration introduces a large pressure gradient in the collision region. In addition, the gas pressure cannot be directly measured at the interaction region. Thus the ionization gauge reading, measured down stream, is a relative pressure measurement. Finally, the pressure gradient along the line of sight makes it difficult to reliably estimate the effective foreground column density of the N_2 emission. The present work finds that the column densities of *Liu et al.* [2005a] and *Ajello et al.* [1989] and, therefore, resonance absorptions, were both underestimated.

[14] To overcome these difficulties with the cross-beam technique, relative intensity measurements were also carried out in swarm mode, where N_2 gas was slowly introduced into, and continuously pumped out of, the collision chamber. Measurement was commenced after a steady equilibrium pressure reading was obtained. While small fluctuations in the N_2 pressure took place during the measurement, they are inconsequential as the pressure at each data point was recorded, along with spectral signal and current, allowing data to be corrected for these fluctuations. The uniform pressure in swarm mode and the absolute pressure reading from the calibrated ionization gauge enable a reliable determination of the N_2 foreground column density from the optical path (~11 cm).

[15] Several e+N_2 emission measurements, at low and high resolution, were carried out at various pressures. A few relative intensity measurements were made with a full-width at half-maximum (FWHM) resolution of ~0.3 Å, in 0.032 Å increments from 935 to 1030 Å. Cross-beam measurements at N_2 background pressures of $\sim 6.7 \times 10^{-6}$, $\sim 3.5 \times 10^{-6}$ and $\sim 1.4 \times 10^{-6}$ Torr, and swarm-mode measurements at $\sim 4.7 \times 10^{-6}$, $\sim 2.5 \times 10^{-6}$ and $\sim 1.1 \times 10^{-6}$ Torr were carried out. For the $c'_4\ ^1\Sigma_u^+(0) - X\ ^1\Sigma_g^+(0)$ band, only the swarm measurements at $\sim 2.5 \times 10^{-6}$ and $\sim 1.1 \times 10^{-6}$ Torr were found to be sufficiently optically thin. On the basis of the (0,0) versus (0,1) band relative intensity measurements at different pressures and configurations, it was found that the cross-beam configuration at $\sim 1.4 \times 10^{-6}$ Torr, utilized for most relative intensity measurements, resulted in a maximum self-absorption of ~3% for the (0,0) band.

[16] The wavelength scale of the measured N_2 emission spectrum was established by assuming a uniform wavelength increment and by using the experimental energy levels reported by *Roncin et al.* [1998, 1999]. The mechanical limitations of the scanning system and slight temperature fluctuations in the spectrometer environment (±0.4°C) during the scan cause non-uniform wavelength drift. The largest wavelength drift, as measured from the extremes, is ~16 mÅ, depending on experimental conditions. The drift is noticeable in high-resolution scans with very long (>300 s per channel) integration times. Except for the high-resolution measurement of the (0,1) band, most of the data were taken with a typical integration time of 5 s per channel and a total of between 30 and 120 repetitive scans across the wavelength region of interest. Data were corrected for the pressure and current variations at each point, followed by summation of the individual scans. High-resolution measurements over short wavelength regions at significantly higher pressure were also made for the (0,1) and (0,2) bands. A spectral resolution of ~33–36 mÅ FWHM was obtained in the high-resolution measurements by operating the spectrometer in second order with ~20 μm slit widths. The wavelength increment was either 4 or 8 mÅ.

[17] An electron-impact-induced emission spectrum of H_2 was also taken to determine the variation of the instrumental spectral sensitivity. The e+H_2 calibration standard and procedure have been discussed in detailed by *Liu et al.* [1995], *Abgrall et al.* [1997], and *Jonin et al.* [2000]. Since these descriptions were published, significant refinements in the e+H_2 calibration standard have been made, including more accurate accounting for the cascade excitation of the $B'\ ^1\Sigma_u^+$, $C\ ^1\Pi_u$, $B'\ ^1\Sigma_u^+$, and $D\ ^1\Pi_u$ states from the higher singlet *gerade* states such as $EF\ ^1\Sigma_g^+$, $GK\ ^1\Sigma_g^+$, $H\bar{H}\ ^1\Sigma_g^+$, $P\ ^1\Sigma_g^+$, $O\ ^1\Sigma_g^+$, $I\ ^1\Pi_g$ and $J\ ^1\Delta_g$ *Liu et al.* [2002, 2003], as well as utilization of the $B''\ ^1\Sigma_u^+ - X\ ^1\Sigma_g^+$ and $D'\ ^1\Pi_u - X\ ^1\Sigma_g^+$ transition probabilities calculated by *Abgrall and Roueff* [2003, private communication]. Emission from the $B\ ^1\Sigma_u^+$, $C\ ^1\Pi_u$, $B'\ ^1\Sigma_u^+$, and $D\ ^1\Pi_u$ states contribute ~95% of the total observed intensities between 900 and 1040 Å, with the remainder from higher ($n \geq 4$) Rydberg states *Jonin et al.* [2000]. The inclusion of the $B''\ ^1\Sigma_u^+ - X\ ^1\Sigma_g^+$ and $D'\ ^1\Pi_u - X\ ^1\Sigma_g^+$ transitions enables the model to reproduce accurately ~99% of the intensities in the region, which reduces the error in the relative sensitivity calibration for the 930–1030 Å region to ≤5%.

3. Theory

3.1. Electron-Impact-Induced Emission

[18] The volumetric photon emission rate I from electron-impact excitation is equal to the excitation rate and the emission branching ratio [*Shemansky et al.*, 1985; *Liu et al.*, 2003]:

$$I(v_j, v_i; J_j, J_i) = g(v_j; J_j)\frac{A(v_j, v_i; J_j, J_i)}{A(v_j; J_j)}, \tag{1}$$

where v and J refer to vibrational and rotational quantum numbers, $A(v_j, v_i; J_j, J_i)$ is the Einstein spontaneous transition probability for emission from level (v_j, J_j) to level (v_i, J_i), and $A(v_j, J_j)$ is the total transition probability (including non-radiative processes) for level (v_j, J_j). In the present study, collision deactivation is negligible, with predissociation the only significant non-radiative process.

[19] The excitation rate $g(v_j; J_j)$ is proportional to the population of molecular nitrogen in the initial level, $N(v_i, J_i)$, the excitation cross section σ, and the electron flux F_e:

$$g(v_j; J_j) = F_e \sum_i N_i \sigma(v_i, v_j; J_i, J_j). \tag{2}$$

For a dipole-allowed transition, the cross section σ_{ij} is related to the absorption oscillator strength and experimental excitation shape function. In the modified Born approximation, the excitation cross section is given by [*Shemansky et al.*, 1985; *Liu et al.*, 2003]:

$$\frac{\sigma_{ij}}{\pi a_0^2} = 4f(v_i, v_j; J_i, J_j)\frac{\mathrm{Ry}}{E_{ij}}\frac{\mathrm{Ry}}{E}\left[\frac{C_0}{C_7}\left(\frac{1}{X^2} - \frac{1}{X^3}\right) + \sum_{k=1}^{4}\frac{C_k}{C_7}(X-1)\exp(-kC_8X) + \frac{C_5}{C_7} + \frac{C_6}{C_7}\frac{1}{X} + \ln(X)\right], \tag{3}$$

where

$$C_7(v_i, v_j; J_i, J_j) = \frac{4\pi a_0^2(2J_i+1)\mathrm{Ry}}{E_{ij}} f(v_i, v_j; J_i, J_j), \tag{4}$$

a_0 and Ry are the Bohr radius and Rydberg constant, respectively, $f(v_i, v_j; J_i, J_j)$ is the absorption oscillator strength, E_{ij} is the transition energy from (v_i, J_i) to (v_j, J_j), E is the electron impact energy, and $X = E/E_{ij}$. The collision strength coefficients C_k/C_7 ($k = 0$–6) and C_8 for the $c'_4\ ^1\Sigma_u^+$ and $b\ ^1\Pi_u - X\ ^1\Sigma_g^+$ band systems have been measured experimentally by *Ajello et al.* [1989] and *James et al.* [1990].

[20] Equation (1) shows that the relative intensities of transitions from the particular rovibrational level (v_j, J_j) to various lower levels (v_i, J_i) is proportional to the relative values of the corresponding line transition probabilities, $A(v_j, v_i; J_j, J_i)$, which are related to the corresponding absorption oscillator strengths $f(v_i, v_j; J_i, J_j)$ by [*Abgrall and Roueff*, 2006]:

$$A(v_j, v_i; J_j, J_i) = 0.667 \times \frac{2J_i+1}{2J_j+1}\nu_{ij}^2 f(v_i, v_j; J_i, J_j) \tag{5}$$

where ν_{ij} refers to the transition frequency in wave numbers.

[21] When band emission from a common vibronic level is considered, the sum of individual ro-vibronic transitions is required. In this case, the $A(v_j; J_j)$ term in Equation (1) has an influence on the relative intensities, specifically through the inherent J_j dependences of both the radiative and non-radiative molecular processes. However, while the significant J_j dependence of predissociation in $c'_4\ ^1\Sigma_u^+(0)$ influences the relative intensities of the rotational lines in each $c'_4\ ^1\Sigma_u^+(0) - X\ ^1\Sigma_g^+$ emission band, it has a negligible (<1%) effect on the relative emission band intensities, which are the principal subject of this study.

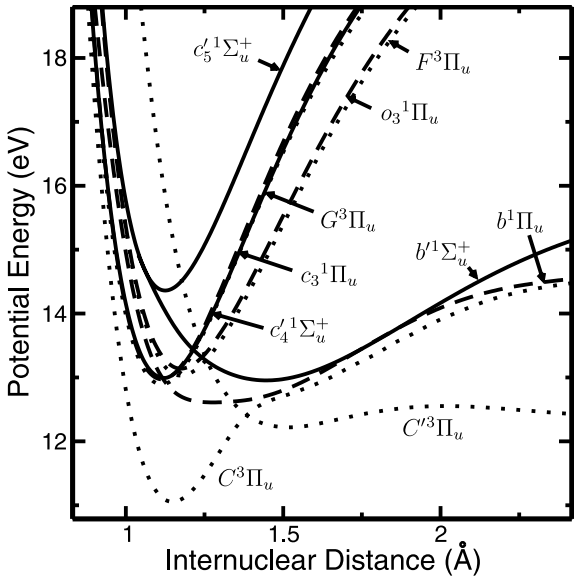

Figure 1. Model diabatic potential-energy curves for the electronic states of N_2 relevant to the present study, relative to the energy of the ground-state $X\ ^1\Sigma_g^+$ potential minimum (not shown). Solid curves: $^1\Sigma_u^+$ states. Dashed curves: $^1\Pi_u$ states. Dotted curves: $^3\Pi_u$ states.

3.2. CSE Molecular Model

[22] In order to obtain a realistic theoretical description of the emission from $c'_4\ ^1\Sigma_u^+(0)$, it is necessary to consider a wide range of excited electronic states and their interactions. Intensities for the allowed transitions of N_2 are affected, not only by the Rydberg-valence interactions within the $^1\Sigma_u^+$ manifold, but also by the rotational coupling between the dipole-accessible $^1\Sigma_u^+$ and $^1\Pi_u$ manifolds, responsible for the *P*/*R*-branch interference effects [*Lefebvre-Brion and Field*, 2004], together with the Rydberg-valence and Rydberg-Rydberg interactions within the $^1\Pi_u$ manifold. Furthermore, Rydberg-valence and Rydberg-Rydberg interactions within the $^3\Pi_u$ manifold, together with the $^1\Pi_u \sim {}^3\Pi_u$ spin-orbit coupling, must be considered if it is hoped to explain the predissociation of any allowed excited N_2 level, which is caused, ultimately, by repulsive $^3\Pi_u$ states. Here, we employ a diabatic-basis coupled-channel Schrödinger equation method to treat all of these interactions.

[23] The formalism of the CSE method has been detailed, e.g., by *van Dishoeck et al.* [1984]. Briefly, for each energy, rotational quantum number, and *e*/*f*-parity [*Lefebvre-Brion and Field*, 2004] of interest, the radial Schrödinger equation for the coupled excited states is solved numerically, yielding coupled-channel wave functions, which are combined with the ground-state radial wave function and appropriate diabatic electronic transition moments, in order to form the total photodissociation cross section. By including centrifugal terms in the ground- and excited-state Hamiltonians, the rotational dependence of the cross section can be evaluated. Transition energies, rotational constants, oscillator strengths, and predissociation linewidths, deduced from the computed CSE cross sections by the fitting of Fano profiles, are compared iteratively with an experimental database using a least squares procedure, in order to optimize the CSE-model parameters, namely the diabatic potential-energy curves, couplings, and electronic transition moments.

[24] The present CSE model of N_2, which remains under development, represents an extension of previous $^{1,3}\Pi_u$-state models [*Lewis et al.*, 2005a; *Haverd et al.*, 2005] to include the $^1\Sigma_u^+$ states necessary to treat the current problem of the $c'_4\ ^1\Sigma_u^+(0)$ emission spectrum. Diabatic potential-energy curves for the ten excited electronic states included in the current model are shown in Figure 1. The *b*, c_3, and $o_3\ ^1\Pi_u$ potentials, and their mutual electrostatic coupling, together with the $X\ ^1\Sigma_g^+$ ground-state potential, are taken from *Lewis et al.* [2005a] while the *C* and $C'\ ^3\Pi_u$ potentials and coupling differ marginally from those of *Lewis et al.* [2005a], due to the inclusion of the *F* and *G* $^3\Pi_u$ Rydberg states in the model. This extended $^3\Pi_u$ model, which has only a minor effect on the emission from high rotational levels of $c'_4\ ^1\Sigma_u^+(0)$, is described in detail elsewhere [*Lewis et al.*, 2007].

[25] The dominant concern when modeling the $^1\Sigma_u^+$ manifold of states is the electrostatic coupling between the $b'\ ^1\Sigma_u^+$ valence state and the two Rydberg states, c'_4 and c'_5 $^1\Sigma_u^+$. The strength of this interaction causes every vibrational level to be homogeneously perturbed by several of its neighbors, meaning that any attempt to reproduce the band spectra with an uncoupled model will fail. The diabatic modeling of *Stahel et al.* [1983] and superseding ab initio work of *Spelsberg and Meyer* [2001] successfully reproduced the $^1\Sigma_u^+$ vibrational energies and rotational constants over a large energy range. Further improvements have been made here by refining the form of the diabatic potential energy curves, shown in Figure 1, and including heterogenous coupling to the $^1\Pi_u$ manifold, necessary to describe *e*-parity energy levels of the rotating molecule.

[26] To represent the homogeneous $b'\ ^1\Sigma_u^+ \sim c'_4\ ^1\Sigma_u^+$ diabatic coupling, the *R*-dependent function of *Spelsberg and Meyer* [2001] has been adopted and rescaled slightly by a factor of 0.95 to better reproduce the experimental energies. A difference in the assumed diabatic viewpoint from that of *Spelsberg and Meyer* [2001] is that the c'_4 and $c'_5\ ^1\Sigma_u^+$ Rydberg states are here assumed to be noninteracting. As discussed further in section 4, the different rotational constants for $b'\ ^1\Sigma_u^+(1)$ and $c'_4\ ^1\Sigma_u^+(0)$ result in a level crossing near $J = 10$, with consequent large energy perturbations. This crossing thus provides a sensitive means of optimizing the scaling factor for the $b' \sim c'$ diabatic coupling.

[27] The heterogeneous $^1\Sigma_u^+ \sim {}^1\Pi_u^e$ interactions, of the form $-\frac{1}{2\mu R^2}H_{\mathrm{JL}}\sqrt{J(J+1)}$, where μ is the N_2 reduced mass, influence principally the energies of high-*J* levels of the $^1\Sigma_u^+$ states and the corresponding $^1\Pi_u^e$ component of Λ-doubling, together with the rotationally dependent *P*- and *R*-branch intensity ratios. The $c'_4\ ^1\Sigma_u^+(0) \sim c_3\ ^1\Pi_u(0)$, $b'\ ^1\Sigma_u^+(3) \sim o_3\ ^1\Pi_u(0)$, and $b'^1\Sigma_u^+(0) \sim b\ ^1\Pi_u(4)$ level crossings are particularly sensitive to heterogeneous interactions. By fitting the CSE-model results to both the *e*- and *f*-parity experimental databases, optimized heterogeneous matrix elements H_{JL} of 2.00, −0.62, and −0.2 cm^{-1}, respectively, were found for the $c'_4\ ^1\Sigma_u^+ \sim c_3\ ^1\Pi_u$, $b'^1\Sigma_u^+ \sim o_3\ ^1\Pi_u$, and $b'\ ^1\Sigma_u^+ \sim b\ ^1\Pi_u$ interactions. The first of these values is consistent with expectation for the interacting members of a 3*p*-Rydberg complex [*Lefebvre-Brion and Field*, 2004].

[28] The R-dependences of the CSE-model diabatic electronic transition moments were taken from *Spelsberg and Meyer* [2001], except for the $c'_4\ ^1\Sigma_u^+ - X\ ^1\Sigma_g^+$ moment, which has been determined specifically using the new photo-emission measurements presented here and is discussed further in section 4. The absolute oscillator strength measurements of *Stark et al.* [2005, 2008] have been used to determine scaling factors, relative to the results of *Spelsberg and Meyer* [2001], for the $b'\ ^1\Sigma_u^+ - X\ ^1\Sigma_g^+$, $b\ ^1\Pi_u - X\ ^1\Sigma_g^+$, $c_3\ ^1\Pi_u - X\ ^1\Sigma_g^+$ and $o_3\ ^1\Pi_u - X\ ^1\Sigma_g^+$ electronic transition moments, yielding fitted values of 0.83, 0.84, 0.85 and 0.89, respectively. Relative phases of the $^1\Sigma_u^+ - X\ ^1\Sigma_g^+$ and $^1\Pi_u - X\ ^1\Sigma_g^+$ electronic transition moments and the rotational coupling parameters have been determined by requiring the model to reproduce correctly the observed sense of the P/R-branch oscillator-strength interference effects in affected transitions.

[29] Because of the increasing $^1\Pi_u^e$-state admixtures in $c'_4\ ^1\Sigma_u^+(0)$ with J, the $c'_4\ ^1\Sigma_u^+(0) - X\ ^1\Sigma_g^+$ transition intensities are influenced somewhat by the $^1\Pi_u - X\ ^1\Sigma_g^+$ electronic transition moments, especially in the case of the weaker bands. A CSE model employed by *Sprenger et al.* [2004a], with the same R-dependence as assumed here for the $b\ ^1\Pi_u - X\ ^1\Sigma_g^+$ transition moment, was found to reproduce successfully the correct relative oscillator strengths, including interference effects, for $b\ ^1\Pi_u(0\text{-}5) - X\ ^1\Sigma_g^+(0)$ and $b\ ^1\Pi_u(1) - X\ ^1\Sigma_g^+(0\text{-}12)$ transitions of N_2. This reinforces the validity of the current approach and the modeled diabatic $b\ ^1\Pi_u - X\ ^1\Sigma_g^+$ contribution to the $c'_4\ ^1\Sigma_u^+(0) - X\ ^1\Sigma_g^+$ transition intensities. Until extensive "hot-band" intensity information is available for transitions to the other states, particularly $c_3\ ^1\Pi_u$, it is not justified to attempt to optimize the R dependences of the corresponding electronic transition moments beyond those of *Spelsberg and Meyer* [2001].

[30] Model $c'_4\ ^1\Sigma_u^+(0) - X\ ^1\Sigma_g^+(v_i)$ relative emission spectra were calculated for the appropriate rotational temperatures using equations (1)–(4), for comparison with the experimental spectra. The spontaneous radiative transition probabilities $A(v_j = 0, v_i; J_j, J_i = J_j \pm 1)$ were obtained from the corresponding CSE-model oscillator strengths using equation (5), while the nonradiative contribution to the total transition probability $A(v_j = 0; J_j)$ was obtained from the corresponding model predissociation linewidth, Γ_{pre}, in cm^{-1} FWHM, using the relation:

$$A_{\text{pre}}(v_j = 0; J_j) = 1.89 \times 10^{11} \Gamma_{\text{pre}}(v_j = 0; J_j)\ \text{s}^{-1}. \quad (6)$$

4. Results and Discussion

[31] Due to the apparatus-sensitivity and optical-thickness constraints of the experimental measurements, the relative intensities of the $c'_4\ ^1\Sigma_u^+(0) - X\ ^1\Sigma_g^+(v_i)$ bands, which are used here to help refine the adopted $c'_4\ ^1\Sigma_u^+ - X\ ^1\Sigma_g^+$ electronic transition moment, are best obtained from the calibrated intensities of the low-resolution data (~0.3 Å FWHM). The computed CSE-model transition probabilities and predissociation lifetimes are utilized to calculate the electron-impact-induced emission spectrum. After the calculated spectrum is convolved with an appropriate instrumental profile, it is compared with the experimental spectrum. The reliability of the CSE results at the rotational level is further examined by comparison with the high-resolution spectra (~33–36 mÅ FWHM).

[32] The use of low-resolution data for determining the relative intensities has several advantages. First, as relative emission intensities to several v_i levels of the $X\ ^1\Sigma_g^+$ state are required, low-resolution measurements make it possible to scan continuously over the required wavelength range within a reasonable time. In addition, the relatively large slit widths enable the data to be measured at lower N_2 pressures (i.e., wider slits compensate for the reduction in intensity due to the lower pressure), eliminating complications due to self-absorption of the (0,0) band. Furthermore, it permits the data points to be acquired over shorter integration times, which in turn reduces the degree of non-uniform wavelength drift caused by small variations in room temperature. Importantly, the use of integrated band intensities ensures that small non-uniform wavelength drifts during the measurement will not have any significant impact on the relative intensity.

[33] The transitions from atomic nitrogen and the N_2 $b'\ ^1\Sigma_u^+(1, 4, 7, 10)$, $b\ ^1\Pi_u(2, 11)$, $c_3\ ^1\Pi_u(1)$, and $o_3\ ^1\Pi_u(4)$ states overlap with some of the $c'_4\ ^1\Sigma_u^+(0) - X\ ^1\Sigma_g^+$ transitions and thus can contribute to the measured band intensities. The atomic nitrogen $2s2p^4\ ^2D - 2s^22p^3\ ^2D^o$ transition, at 980.632 and 980.706 Å, overlaps with the (0,1) band. Because of the homogeneous coupling between $b'\ ^1\Sigma_u^+(1)$ and $c'_4\ ^1\Sigma_u^+(0)$, and their associated level crossing, the contribution of the $b'\ ^1\Sigma_u^+(1) - X\ ^1\Sigma_g^+(v_i)$ emissions is always significant, at least for the J_j = 8-12 levels. The $c_3\ ^1\Pi_u(1) - X\ ^1\Sigma_g^+(v_i{+}1)$ emissions overlap the longer-wavelength regions (P-branch) of the $c'_4\ ^1\Sigma_u^+(0) - X\ ^1\Sigma_g^+(v_i)$ bands. Furthermore, the predissociation rate of $c_3\ ^1\Pi_u(1)$ increases rapidly with J_j [*Kawamoto et al.*, 1997; *Sprengers et al.*, 2004b; *Sprengers and Ubachs*, 2006]. The $b'\ ^1\Sigma_u^+(7) - X\ ^1\Sigma_g^+(v_i{+}2)$ band can also overlap the shorter-wavelength regions (R-branch) of the $c'_4\ ^1\Sigma_u^+(0) - X\ ^1\Sigma_g^+(v_i)$ bands transition. Other potential overlapping transitions include the $b'\ ^1\Sigma_u^+(4) - X\ ^1\Sigma_g^+(v_i{+}1)$, $b'\ ^1\Sigma_u^+(10) - X\ ^1\Sigma_g^+(v_i{+}3)$, $b\ ^1\Pi_u(2) - X\ ^1\Sigma_g^+(v_i{-}1)$, and $b\ ^1\Pi_u(11) - X\ ^1\Sigma_g^+(v_i{+}2)$ bands. However, their contributions are generally negligible, either because of strong predissociation, or because of small excitation cross sections from the $X\ ^1\Sigma_g^+(0)$ state. In any case, the relative importance of these overlapping transitions increases with v_i due to the rapid decrease of the $c'_4\ ^1\Sigma_u^+(0) - X\ ^1\Sigma_g^+(v_i)$ band intensities. The contributions of the above mentioned bands were taken into account by using either the CSE-model or experimental oscillator strengths and predissociation rates. The more prominent overlapping transitions will be discussed later, together with the analysis of the high-resolution spectra.

[34] Figure 2 compares the calibrated low-resolution experimental spectra with the corresponding CSE-model spectra in the neighborhoods of the $c'_4\ ^1\Sigma_u^+(0) - X^1\Sigma_g^+(0{-}3)$ bands. At the low pressures needed to achieve nearly optically thin conditions for the (0,0) band, N_2 molecules suffer very little rotational cooling. Consequently, a temperature of 300 K has been used in calculations of the CSE-model spectra. The CSE-model calculations reproduce well the relative intensities and spectral shapes of the (0,0), (0,1) and (0,2) bands in the low-resolution spectra,

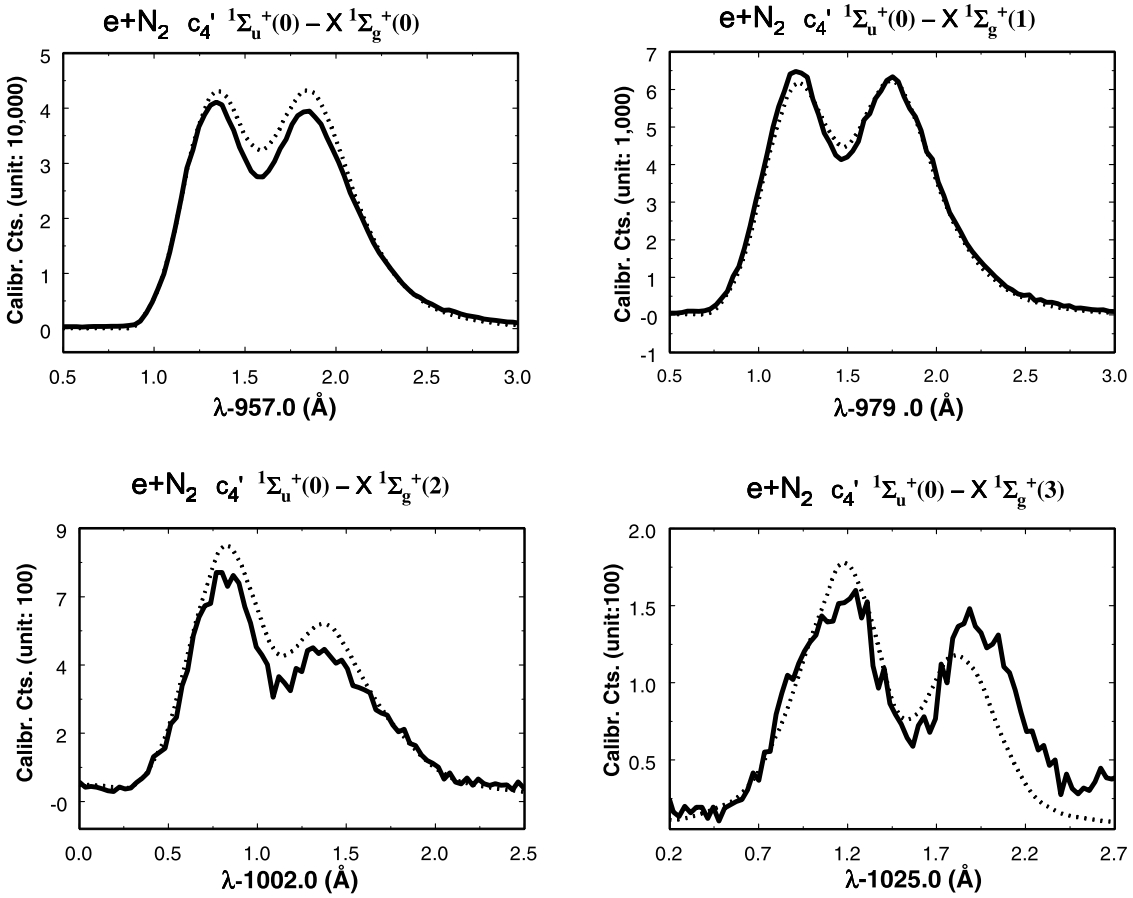

Figure 2. Comparison of calibrated experimental (solid lines) and CSE-model (dotted lines) e + N_2 low-resolution emission spectra for the $c'_4\ ^1\Sigma_u^+(0) - X\ ^1\Sigma_g^+(0-3)$ transitions. The experimental spectra were obtained concurrently in cross-beam mode, with 100 eV excitation energy and a spectral resolution of ~0.3 Å FWHM. The model spectra were generated assuming a rotational temperature of 300 K. All y-axes refer to calibrated intensity in counts, with appropriate indicated scales, while all x-axes refer to wavelength in Å, with indicated offsets. An upper limit of 3% was estimated for the resonance absorption in the $c'_4\ ^1\Sigma_u^+(0) - X\ ^1\Sigma_g^+(0)$ band, i.e., had the resonance absorption been absent, the solid trace for the $c'_4\ ^1\Sigma_u^+(0) - X\ ^1\Sigma_g^+(0)$ transition would have been $\leq$3% stronger. The emission intensity drops by a factor of ~300 from $v_i = 0$ to $v_i = 3$. See section 4 for a discussion of the discrepancy for $\lambda \geq$ 1026.6 Å.

validating the CSE treatment of the $c'_4\ ^1\Sigma_u^+$ state and its coupling. For the (0,3) band, which is weaker than the (0,0) band by a factor of ~300 and the measured intensity has an estimated uncertainty of ~18%, mainly because of the relatively large uncertainty in the background subtraction, intensities on the *R*-branch (shorter-wavelength) side are reproduced to within the experimental uncertainty. However, the model underestimates significantly the intensity on the *P*-branch (long-wavelength) side of this band. While the reason for this is not clear, it is most likely due to weak atomic nitrogen emission that is not included in the current model, since the discrepancy applies only to one side of the band. Emission from the $b'\ ^1\Sigma_u^+(1)$ state is unlikely to be responsible, since it is known to be weak in this region, and, in any case, the $b'\ ^1\Sigma_u^+ - X\ ^1\Sigma_g^+$ electronic transition moment employed in the CSE model is well constrained by the experimental oscillator strengths for the $b'\ ^1\Sigma_u^+(v_j) - X\ ^1\Sigma_g^+(0)$ bands [*Stark et al.*, 2000, 2008]. As mentioned above, the $c_3\ ^1\Pi_u(1) - X\ ^1\Sigma_g^+(v_i{+}1)$ band emissions overlap with the *P*-branch side of the $c'_4\ ^1\Sigma_u^+(0) - X\ ^1\Sigma_g^+(v_i)$ band emissions, and, indeed, the $c_3\ ^1\Pi_u(1) - X\ ^1\Sigma_g^+(4)$ band lies in the correct position to explain the additional emission on the *P*-branch side of the $c'_4\ ^1\Sigma_u^+(0) - X\ ^1\Sigma_g^+(3)$ band. However, the calculated emission, which is included in the model spectrum of Figure 2, is too weak to fully explain the discrepancy. In principle, a change to the *R*-dependence of the model $c_3\ ^1\Pi_u - X\ ^1\Sigma_g^+$ electronic transition moment might improve matters, but, considering that good agreement is found between the model and experimental spectra for the $c_3\ ^1\Pi_u(1) - X\ ^1\Sigma_g^+(0)$ band, and that the model $c_3\ ^1\Pi_u(1) - X\ ^1\Sigma_g^+(3)$ band emission is somewhat too large compared with experiment, it is unlikely that a realistic *R*-dependence will simultaneously explain the observations for all three bands. Possible atomic nitrogen emissions in the region are the $2s^22p^2(^3P)12d^2D - 2s^22p^3\ ^2D^o_{5/2}$ and $2s^22p^2(^3P)12d\ ^2D - 2s^22p^3\ ^2D^o_{3/2}$ transitions, at 1026.69 and 1026.78 Å, respectively, and spin-forbidden transitions, $2s^22p^2(^3P)12d\ ^4P - 2s^22p^3\ ^2D^o_{5/2}$ and $2s^22p^2(^3P)12d\ ^4P - 2s^22p^3\ ^2D^o_{3/2}$, at 1027.15 and 1027.24 Å, respectively. The $c'_4\ ^1\Sigma_u^+(0) -$

Table 1. Comparison of Experimental and Calculated Relative Emission Intensities for the $c'_4\ ^1\Sigma_u^+$ (0) $- X\ ^1\Sigma_g^+(v_i)$ Transitions of N_2[a]

v_i	Exp.	CSE[b]	CSE-noR[c]	FCF[d]
0	6.3(4)	6.8	7.8	7.3
1	1.0	1.0	1.0	1.0
2	0.099(9)	0.113	0.087	0.085
3	0.019(4)	0.018	0.016	0.003

[a]Normalized to the (0,1) band intensity. Values in parentheses represent experimental uncertainties in units of the least significant digit.
[b]CSE-model results for $T = 300$ K using final $c'_4 - X$ electronic transition moment.
[c]CSE-model results for $T = 300$ K using R-independent $c'_4 - X$ electronic transition moment.
[d]Results of uncoupled rotationless calculation using final $c'_4 - X$ electronic transition moment.

$X\ ^1\Sigma_g^+(3)$ spectrum in Figure 2, however, shows that the spin-allowed atomic nitrogen emissions cannot alone account for the intensity difference. A slightly stronger contribution from the spin-forbidden transitions is required to satisfactorily account for the intensity discrepancy. Unpublished experimental measurements by one of us (JMA) at 20 eV and 100 eV provide strong evidence that both spin-allowed and spin-forbidden atomic nitrogen transitions contribute to the P-branch side of the (0,3) band. Since atomic nitrogen emission is energetically impossible at E $\leq$ 20 eV, a comparison of the emission spectra at 20 and 100 eV enables an unambiguous identification of atomic nitrogen and nitrogen ion emissions when the overlap of the atomic and molecular transitions is negligible. The measurements have shown extensive atomic nitrogen emission from the $n = 3-11$ $2s^22p^2(^3P)nd\ ^2D$, ^2P and ^2F doublet states, and some of the quartet states to the $2s^22p^3\ ^2D^o$ state. In a few cases, the spin-forbidden transitions from the quartet states can be unambiguously identified. For instance, at 100 eV electron energy, the $2s^22p^2(^3P)4d\ ^4D - 2s^22p^3\ ^2D$ spin-forbidden transition, between 1096.747 and 1096.945 Å, has a slightly stronger intensity than the allowed $2s^22p^2(^3P)4d\ ^2D - 2s^22p^3\ ^2D^o$ transition, between 1095.941 and 1096.046 Å. Finally, the tabulation by *Smith et al.* [2001] predicts that the transition probability of the spin-forbidden $2s^22p^2(^3P)12d\ ^4P - 2s^22p^3\ ^2D^o$ transition is actually ~2.7 times greater than that of the allowed $2s^22p^2(^3P)12d\ ^2D - 2s^22p^3\ ^2D^o$ transition. In any case, it is important to note that the transitions near the $c'_4\ ^1\Sigma_u^+(0) - X\ ^1\Sigma_g^+(3)$ band contribute <0.4% of the total emission intensity from the $c'_4\ ^1\Sigma_u^+(0)$ level. Thus the ~40% difference between the experimental and calculated P-branch side intensities for this band represents<0.1% of the total.

[35] In Table 1, a comparison is made between the experimental and CSE-model relative emission intensities for the $c'_4\ ^1\Sigma_u^+(0) - X\ ^1\Sigma_g^+(v_i = 0\text{-}3)$ bands of N_2, normalized with respect to the (0,1) -band value. The experimental values were obtained by integration of the $T = 300$ K spectra in Figure 2, with a 3% correction to allow for the effects of self-absorption on the (0,0) -band intensity, and further small corrections applied for the contributions of known overlapping N_2 features. The CSE-model relative intensities (column three of Table 1) are in overall very good agreement with the experimental values, the maximum discrepancy of 14%, occurring for the (0,2) band, representing less than two standard deviations. CSE-model intensities, computed in the same way, but assuming no R dependence in the $c'_4\ ^1\Sigma_u^+ - X\ ^1\Sigma_g^+$ electronic transition moment (column four of Table 1), are seen to be in significantly worse agreement with experiment, with deviations changing systematically from +22% for $v_i = 0$, to -15% for $v_i = 3$. Thus the experimental relative intensities confirm that an R dependence is needed in the transition moment. In addition, for comparison we have computed simplistic relative intensities using the final CSE-model parameters, but assuming that the diabatic $c'_4\ ^1\Sigma_u^+$ state is *uncoupled* (final column of Table 1). The results of this Franck-Condon-like model are also in very poor agreement with experiment, with deviations changing systematically from +16% for $v_i = 0$, to −84% for $v_i = 3$. This demonstrates unambiguously that Franck-Condon models are of little use in the interpretation of the N_2 spectrum in this region where strong coupling is endemic, requiring the use of the CSE method.

[36] Further validation of the CSE model is provided in Table 2, where a comparison is made between the $c'_4\ ^1\Sigma_u^+(v_j = 0-3) - X\ ^1\Sigma_g^+(0)$ bands of N_2. For simplicity, this comparison is made in terms of the rotationless oscillator strengths, with the experimental values having been extrapolated to $J_j = J_i = 0$ [*Stark et al.*, 2005, 2008]. The final CSE-model values (column three of Table 2) are in excellent agreement with experiment, with a maximum discrepancy of <10%. In comparison, CSE-model values calculated assuming no R dependence in the $c'_4\ ^1\Sigma_u^+ - X\ ^1\Sigma_g^+$ electronic transition moment (final column of Table 2) can be scaled to provide only marginally worse agreement with experiment. Thus it can be concluded that the relative $(0,v_i)$ intensities measured here provide a significantly more sensitive measure of the transition-moment R dependence than do the $(v_j,0)$ oscillator strengths.

[37] The range of R over which the $c'_4\ ^1\Sigma_u^+ - X\ ^1\Sigma_g^+$ electronic transition moment significantly influences the oscillator strengths considered here has been determined by comparing CSE-model oscillator strengths for various degrees of truncation of the transition-moment function. A range of 1.05–1.22 Å was found for the (0,0) band, increasing to 1.00–1.27 Å for the (0,3) band. The adopted CSE-model diabatic $c'_4\ ^1\Sigma_u^+ - X\ ^1\Sigma_g^+$ electronic transition moment, in a.u., has the form:

$$M(R) = -0.4702 - 6.620(R - 1.068)^2;\ 1.00 < R < 1.27\ \text{Å} \tag{7}$$

Table 2. Comparison of Experimental and Calculated Rotationless Oscillator Strengths for the $c'_4\ ^1\Sigma_u^+(v_j) - X\ ^1\Sigma_g^+(0)$ Bands of N_2

v_j	Exp.	CSE[a]	CSE-noR[b]
0	0.138(14)[c]	0.138	0.138
1	0.0052(6)[c]	0.0054	0.0063
2	0.0012(1)[d]	0.0011	0.0011
3	0.0076(7)[d]	0.0081	0.0080

[a]CSE-model results using final $c'_4 - X$ electronic transition moment.
[b]CSE-model results using R-independent $c'_4 - X$ electronic transition moment.
[c]Fitted rotationless oscillator strengths of *Stark et al.* [2005].
[d]Fitted rotationless oscillator strengths of *Stark et al.* [2008].

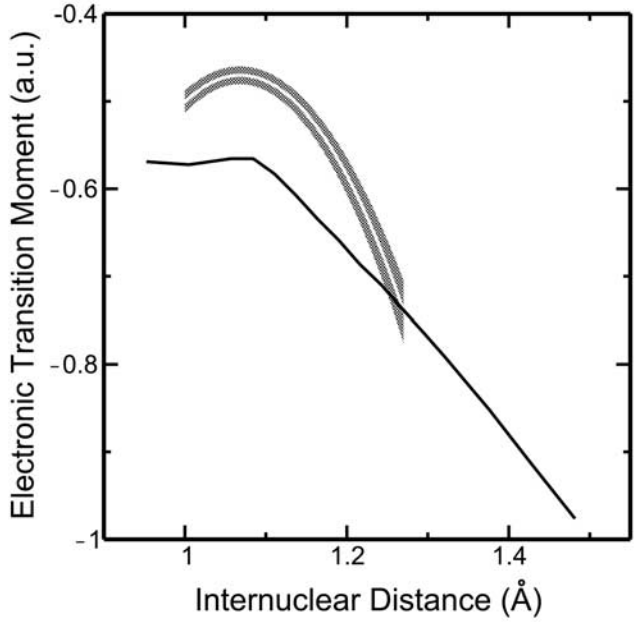

Figure 3. Adopted CSE-model diabatic $c'_4\ ^1\Sigma_u^+ - X\ ^1\Sigma_g^+$ electronic transition moment (white curve), including uncertainty range (shaded area), compared with ab initio calculation of *Spelsberg and Meyer* [2001] (black curve).

The reader is cautioned against using equation (7) for *R*-values outside its range of applicability. In such regions, the *R* dependence calculated ab initio by *Spelsberg and Meyer* [2001] is likely to be significantly more realistic. The CSE-model transition moment is compared with that of *Spelsberg and Meyer* [2001] in Figure 3. While the general forms of the transition moments are similar, the average magnitude of the adopted CSE moment is ~15% less than the ab initio value. Discrepancies of similar magnitude and sign have been found in the case of the diabatic transition moments for the b, c_3, and $o_3\ ^1\Pi_u - X\ ^1\Sigma_g^+$ transitions of N_2 [*Haverd et al.*, 2005].

[38] The CSE-model calculated line transition probabilities for the $c'_4\ ^1\Sigma_u^+(0) - X\ ^1\Sigma_g^+(0-3)$ and $b'\ ^1\Sigma_u^+(1) - X\ ^1\Sigma_g^+(0-3)$ bands are listed in Tables 5 and 6, respectively, along with the estimated total *radiative* transition probabilities of the $c'_4\ ^1\Sigma_u^+(0)$ and $b'\ ^1\Sigma_u^+(1)$ levels, obtained by summing line transition probabilities up to $v_i = 29$ of the $X\ ^1\Sigma_g^+$ state. The transition frequencies of $c'_4\ ^1\Sigma_u^+(0) - X\ ^1\Sigma_g^+(0-3)$ and $b'\ ^1\Sigma_u^+(1) - X\ ^1\Sigma_g^+(0\text{-}3)$ bands are listed in Tables 5 and Table 6. In the case of the $c'_4\ ^1\Sigma_u^+(0) - X\ ^1\Sigma_g^+(v_j)$ transition, the listed bands represent the strongest emissions from the $c'_4\ ^1\Sigma_u^+(0)$ level. Because the potential-energy curve for the diabatic $c'_4\ ^1\Sigma_u^+$ state is very similar to that of the $X\ ^1\Sigma_g^+$ state, the diabatic Franck-Condon factor for the $c'_4\ ^1\Sigma_u^+(0) - X\ ^1\Sigma_g^+(0)$ band is on the order of 0.9 [*Stahel et al.*, 1983; *Whang et al.*, 1996]. Thus a very substantial proportion of the $c'_4\ ^1\Sigma_u^+ - X\ ^1\Sigma_g^+$ electron-impact excitation normally ends up in the $c'_4\ ^1\Sigma_u^+(0)$ level, with most emission back to the $X\ ^1\Sigma_g^+(0)$ level. The diabatic $b'\ ^1\Sigma_u^+(1) - X\ ^1\Sigma_g^+(0-2)$ Franck-Condon factors are very small, but rotational lines involving $b'\ ^1\Sigma_u^+(1)$ levels in the region of the $b'\ ^1\Sigma_u^+(1) \sim c'_4\ ^1\Sigma_u^+(0)$ level crossing borrow significant strength from the corresponding $c'_4\ ^1\Sigma_u^+(0) - X\ ^1\Sigma_g^+(0\text{-}2)$ transitions, through the $b'\ ^1\Sigma_u^+(1) \sim c'_4\ ^1\Sigma_u^+(0)$ homogeneous coupling. The overall $b'\ ^1\Sigma_u^+(1) - X\ ^1\Sigma_g^+(v_i)$ emission becomes more significant in the far-ultraviolet region. Estimated uncertainties in the calculated transition probabilities for the strong and moderately strong transitions in Tables 3 and 4 are $\leq$12%.

[39] The accuracy of the line transition probabilities listed in Tables 3 and 4 can be examined for each band. Reliable absolute transition probabilities for the $b'\ ^1\Sigma_u^+(1) - X\ ^1\Sigma_g^+(0)$ and $c'_4\ ^1\Sigma_u^+(0) - X\ ^1\Sigma_g^+(0)$ bands can be inferred from the high-resolution photoabsorption experiments of *Stark et al.* [2000]. Of the 64 measured *P*- and *R*-branch transitions, 57 calculated transition probability values agree with the experimental ones within the experimental uncertainties. All remaining 7 transitions agree within twice the experimental uncertainties. Overall, the agreement for the *R*-branch transitions is better than for the *P* branches, where the calculated values are generally smaller than their experimental counterparts.

[40] In the case of the (0,1) and (0,2) bands, where no absolute experimental data exist, apart from those inferred indirectly from the present work, the relative CSE-model line intensities can be compared with those from the high-resolution experimental spectra. Because of the J_j-dependent predissociation of the $c'_4\ ^1\Sigma_u^+(0)$ levels [*Ubachs et al.*, 2001; *Liu et al.*, 2005a], the calculated relative emission intensity depends somewhat on the predissociation rate for each J_j level. *Ubachs et al.* [2001] measured the lifetimes of several groups of unresolved J_j levels of the $c'_4\ ^1\Sigma_u^+(0)$ state in the time domain. By interpolation and extrapolation of the results of *Ubachs et al.* [2001], *Liu et al.* [2005a] derived a set of lifetimes in order to analyze the emission spectrum of the $c'_4\ ^1\Sigma_u^+(0) - X\ ^1\Sigma_g^+(0)$ band. As shown by *Lewis et al.* [2005a, 2005b], the predissociation rate can also be computed using the CSE model. The predissociation rates and lifetimes for various rotational levels of the $c'_4\ ^1\Sigma_u^+(0)$ state will be examined in a future joint experimental and theoretical paper. It is sufficient to point out here that a set of lifetimes, estimated from the preliminary CSE predissociation linewidths provided by the current model, has been used to aid the calculation of the emission spectra. These CSE lifetimes are consistent with those of *Liu et al.* [2005a] for $J_j \leq 20$. For $J_j > 20$, the estimated CSE lifetimes are somewhat longer, leading to greater calculated emission intensities. The differences in overall relative intensities, however, are small because emissions from levels with $J_j > 20$ are weak. The primary effect is that the estimated CSE lifetime leads to a slightly lower inferred rotational temperature [e.g., 260 K versus 270 K for the (0,1) band].

[41] Figures 4 and 5 compare experimental and CSE-model emission spectra at the rotational level for the $c'_4\ ^1\Sigma_u^+(0) - X\ ^1\Sigma_g^+(1)$ and $c'_4\ ^1\Sigma_u^+(0) - X\ ^1\Sigma_g^+(2)$ bands, respectively. Higher backing N_2 pressures were utilized in the experiments to compensate for the decrease in the (0,1) and (0,2) band emission intensities. The increase in rotational cooling results in temperatures of ~260 and ~150 K, respectively, for the high-resolution spectra of the (0,1) and (0,2) bands. With an N_2 pressure of $(0.9\sim0.1) \times 10^{-4}$ Torr and 20 μm slit widths (in second order), the (0,1) band emission remains reasonably strong, and a single scan with an integration time of ~220 s per channel and ~14.5 h total acquisition time is sufficient. As a result, only very small

Table 3. Transition Probabilities of the $c'_4\ ^1\Sigma_u^+(0) - X\ ^1\Sigma_g^+(v_i)$ ($v_i = 0–3$) Bands (s^{-1})[a]

		$c'_4\ ^1\Sigma_u^+(0) - X\ ^1\Sigma_g^+(0)$		$c'_4\ ^1\Sigma_u^+(0) - X\ ^1\Sigma_g^+(1)$		$c'_4\ ^1\Sigma_u^+(0) - X\ ^1\Sigma_g^+(2)$		$c'_4\ ^1\Sigma_u^+(0) - X\ ^1\Sigma_g^+(3)$	
J_j	$A_T^e(J_j)$[b]	$R(J_j - 1)$	$P(J_j + 1)$	$R(J_j - 1)$	$P(J_j + 1)$	$R(J_j - 1)$	$P(J_j + 1)$	$R(J_j - 1)$	$P(J_j + 1)$
0	1.172E9		1.00E9		1.48E8		1.65E7		2.24E6
1	1.172E9	3.26E8	6.76E8	4.89E7	9.89E7	5.88E6	1.06E7	8.83E5	1.37E6
2	1.171E9	3.86E8	6.15E8	5.85E7	8.93E7	7.28E6	9.26E6	1.15E6	1.14E6
3	1.170E9	4.09E8	5.92E8	6.24E7	8.54E7	8.05E6	8.55E6	1.34E6	9.96E5
4	1.169E9	4.18E8	5.80E8	6.43E7	8.33E7	8.59E6	8.07E6	1.51E6	8.92E5
5	1.168E9	4.23E8	5.74E8	6.54E7	8.21E7	9.03E6	7.72E6	1.67E6	8.11E5
6	1.166E9	4.24E8	5.70E8	6.59E7	8.14E7	9.42E6	7.45E6	1.85E6	7.48E5
7	1.163E9	4.23E8	5.67E8	6.60E7	8.09E7	9.77E6	7.25E6	2.06E6	7.06E5
8	1.158E9	4.19E8	5.62E8	6.57E7	8.04E7	1.01E7	7.13E6	2.32E6	6.98E5
9	1.144E9	4.09E8	5.48E8	6.44E7	7.91E7	1.04E7	7.09E6	2.71E6	7.70E5
10	1.058E9	3.52E8	4.72E8	5.64E7	6.98E7	1.02E7	6.89E6	3.52E6	1.19E6
11	1.007E9	3.38E8	4.53E8	4.98E7	6.27E7	6.30E6	3.62E6	5.66E5	2.31E4
12	1.128E9	4.09E8	5.47E8	6.13E7	7.83E7	9.00E6	5.38E6	1.64E6	4.53E4
13	1.145E9	4.19E8	5.58E8	6.25E7	8.13E7	9.63E6	5.79E6	2.11E6	8.09E4
14	1.149E9	4.22E8	5.59E8	6.23E7	8.29E7	9.86E6	5.98E6	2.42E6	8.54E4
15	1.148E9	4.24E8	5.57E8	6.16E7	8.41E7	9.92E6	6.13E6	2.67E6	7.73E4
16	1.146E9	4.26E8	5.52E8	6.07E7	8.52E7	9.87E6	6.29E6	2.90E6	6.43E4
17	1.142E9	4.28E8	5.45E8	5.95E7	8.64E7	9.72E6	6.47E6	3.12E6	5.00E4
18	1.136E9	4.31E8	5.36E8	5.80E7	8.75E7	9.48E6	6.69E6	3.33E6	3.62E4
19	1.128E9	4.34E8	5.25E8	5.63E7	8.86E7	9.14E6	6.97E6	3.53E6	2.39E4
20	1.117E9	4.37E8	5.10E8	5.42E7	8.97E7	8.67E6	7.31E6	3.72E6	1.38E4
21	1.101E9	4.41E8	4.90E8	5.17E7	9.06E7	8.05E6	7.73E6	3.90E6	6.40E3
22	1.080E9	4.45E8	4.65E8	4.87E7	9.11E7	7.26E6	8.25E6	4.04E6	1.83E3
23	1.050E9	4.48E8	4.33E8	4.51E7	9.12E7	6.28E6	8.87E6	4.14E6	5.67E1
24	1.009E9	4.49E8	3.92E8	4.07E7	9.02E7	5.12E6	9.62E6	4.14E6	5.25E2
25	9.553E8	4.46E8	3.41E8	3.56E7	8.79E7	3.79E6	1.05E7	4.02E6	1.93E3
26	8.870E8	4.39E8	2.82E8	2.98E7	8.37E7	2.42E6	1.14E7	3.72E6	2.40E3
27	8.047E8	4.24E8	2.18E8	2.37E7	7.74E7	1.20E6	1.24E7	3.24E6	8.70E2
28	7.166E8	4.03E8	1.56E8	1.79E7	6.92E7	3.46E5	1.33E7	2.59E6	4.99E2
29	6.327E8	3.78E8	1.02E8	1.31E7	5.99E7	4.72E3	1.41E7	1.87E6	1.23E4
30	5.461E8	3.51E8	6.01E7	9.32E6	5.05E7	1.83E5	1.47E7	1.18E6	5.53E4

[a] x.yEz = x.y × 10^z.
[b] Total *radiative* transition probability (s^{-1}).

Table 4. Transition Probabilities of the $b'\ ^1\Sigma_u^+$ (1) $- X\ ^1\Sigma_g^+(v_i)$ (v_i = 0–3) Bands (s^{-1})[a]

		$b'\ ^1\Sigma_u^+(1) - X\ ^1\Sigma_g^+(0)$		$b'\ ^1\Sigma_u^+(1) - X\ ^1\Sigma_g^+(1)$		$b'\ ^1\Sigma_u^+(1) - X\ ^1\Sigma_g^+(2)$		$b'\ ^1\Sigma_u^+(1) - X\ ^1\Sigma_g^+(3)$	
J_j	$A_T^e(J_j)$[b]	$R(J_j - 1)$	$P(J_j + 1)$	$R(J_j - 1)$	$P(J_j + 1)$	$R(J_j - 1)$	$P(J_j + 1)$	$R(J_j - 1)$	$P(J_j + 1)$
0	4.923E8		3.15E6		2.81E4		8.00E5		3.62E6
1	4.922E8	1.06E6	2.19E6	1.03E4	2.19E4	2.60E5	5.31E5	1.20E6	2.42E6
2	4.921E8	1.35E6	2.13E6	1.58E4	2.59E4	3.03E5	4.71E5	1.42E6	2.17E6
3	4.918E8	1.59E6	2.27E6	2.41E4	3.57E4	3.10E5	4.37E5	1.50E6	2.06E6
4	4.916E8	1.89E6	2.59E6	3.87E4	5.45E4	3.01E5	4.06E5	1.53E6	1.98E6
5	4.914E8	2.35E6	3.14E6	6.60E4	9.01E4	2.79E5	3.73E5	1.52E6	1.92E6
6	4.915E8	3.10E6	4.11E6	1.21E5	1.61E5	2.43E5	3.31E5	1.49E6	1.87E6
7	4.922E8	4.52E6	5.98E6	2.43E5	3.17E5	1.89E5	2.74E5	1.42E6	1.80E6
8	4.952E8	7.69E6	1.02E7	5.63E5	7.24E5	1.08E5	1.89E5	1.30E6	1.71E6
9	5.071E8	1.74E7	2.32E7	1.71E6	2.17E6	9.84E3	6.11E4	1.03E6	1.55E6
10	5.887E8	7.37E7	9.84E7	9.39E6	1.18E7	4.09E5	1.24E5	3.57E5	1.05E6
11	6.379E8	8.62E7	1.16E8	1.55E7	1.93E7	4.40E6	3.30E6	3.44E6	2.13E6
12	5.151E8	1.53E7	2.06E7	3.44E6	4.24E6	1.77E6	1.48E6	2.50E6	2.03E6
13	4.948E8	5.28E6	7.16E6	1.49E6	1.83E6	1.17E6	1.05E6	2.16E6	1.92E6
14	4.875E8	2.50E6	3.40E6	8.79E5	1.07E6	9.34E5	8.63E5	2.00E6	1.84E6
15	4.834E8	1.40E6	1.90E6	6.03E5	7.32E5	8.04E5	7.62E5	1.89E6	1.78E6
16	4.803E8	8.74E5	1.18E6	4.53E5	5.48E5	7.21E5	6.95E5	1.81E6	1.73E6
17	4.778E8	5.86E5	7.79E5	3.61E5	4.34E5	6.60E5	6.47E5	1.74E6	1.68E6
18	4.754E8	4.15E5	5.41E5	2.99E5	3.58E5	6.13E5	6.08E5	1.68E6	1.64E6
19	4.731E8	3.07E5	3.88E5	2.54E5	3.04E5	5.73E5	5.77E5	1.62E6	1.59E6
20	4.709E8	2.36E5	2.86E5	2.21E5	2.64E5	5.39E5	5.50E5	1.56E6	1.55E6
21	4.687E8	1.89E5	2.14E5	1.96E5	2.32E5	5.08E5	5.26E5	1.51E6	1.51E6
22	4.665E8	1.56E5	1.61E5	1.76E5	2.06E5	4.79E5	5.05E5	1.46E6	1.47E6
23	4.642E8	1.35E5	1.21E5	1.60E5	1.85E5	4.51E5	4.87E5	1.40E6	1.43E6
24	4.620E8	1.22E5	8.92E4	1.47E5	1.67E5	4.24E5	4.71E5	1.34E6	1.39E6
25	4.597E8	1.19E5	6.25E4	1.37E5	1.51E5	3.96E5	4.59E5	1.28E6	1.36E6
26	4.574E8	1.30E5	3.82E4	1.31E5	1.35E5	3.65E5	4.53E5	1.21E6	1.34E6
27	4.552E8	1.75E5	1.38E4	1.32E5	1.20E5	3.25E5	4.61E5	1.12E6	1.34E6
28	4.528E8	4.07E5	4.17E3	1.58E5	9.63E4	2.50E5	5.27E5	9.49E5	1.45E6
29	3.802E8	8.94E7	3.82E7	4.56E6	3.81E5	2.99E6	7.95E6	3.29E6	1.08E7
30	4.479E8	1.11E5	2.89E5	3.14E4	1.37E5	4.66E5	2.06E5	1.41E6	8.15E5

[a] x.yEz = x.y $\times$ 10^z.
[b] Total *radiative* transition probability (s^{-1}).

Table 5. Transition Frequencies of the $c'_4\ ^1\Sigma_u^+(0) - X\ ^1\Sigma_g^+(v_i)$ ($v_i = 0-3$) Bands (cm^{-1})[a]

	$c'_4\ ^1\Sigma_u^+(0) - X\ ^1\Sigma_g^+(0)$		$c'_4\ ^1\Sigma_u^+(0) - X\ ^1\Sigma_g^+(1)$		$c'_4\ ^1\Sigma_u^+(0) - X\ ^1\Sigma_g^+(2)$		$c'_4\ ^1\Sigma_u^+(0) - X\ ^1\Sigma_g^+(3)$	
J_j	$R(J_j-1)$	$P(J_j+1)$	$R(J_j-1)$	$P(J_j+1)$	$R(J_j-1)$	$P(J_j+1)$	$R(J_j-1)$	$P(J_j+1)$
0		104318.5		101988.6		99687.4		97414.9
1	104326.4	104314.5	101996.5	101984.7	99695.2	99683.6	97422.6	97411.2
2	104330.1	104310.2	102000.2	101980.6	99698.9	99679.6	97426.5	97407.1
3	104333.8	104305.9	102003.9	101976.4	99702.8	99675.5	97430.5	97403.2
4	104337.2	104301.4	102007.6	101972.1	99706.6	99671.3	97434.1	97399.3
5	104340.5	104296.7	102011.0	101967.6	99710.0	99667.0	97437.8	97395.2
6	104343.7	104292.0	102014.3	101963.1	99713.6	99662.8	97441.6	97391.2
7	104346.7	104287.0	102017.5	101958.4	99717.0	99658.4	97445.2	97387.1
8	104349.4	104281.7	102020.5	101953.5	99720.2	99653.7	97448.6	97382.7
9	104351.7	104276.1	102023.1	101948.1	99723.1	99648.8	97451.7	97378.1
10	104353.0	104269.5	102024.7	101941.9	99725.0	99643.0	97454.0	97372.8
11	104360.1	104268.6	102032.1	101941.4	99732.8	99642.9	97462.1	97373.2
12	104360.5	104261.5	102032.9	101934.4	99734.0	99636.4	97463.8	97367.0
13	104361.8	104254.3	102034.6	101928.3	99736.1	99630.7	97466.4	97361.9
14	104363.4	104247.6	102036.3	101922.1	99738.3	99625.1	97468.9	97356.6
15	104364.1	104241.0	102038.0	101915.9	99740.5	99619.4	97471.6	97351.6
16	104365.0	104234.0	102039.4	101909.6	99742.4	99613.5	97474.0	97346.5
17	104365.3	104226.4	102040.1	101902.4	99743.6	99607.0	97475.9	97340.5
18	104365.6	104219.1	102041.2	101895.5	99745.2	99600.9	97478.1	97335.1
19	104365.2	104210.3	102041.2	101887.8	99745.9	99593.9	97479.4	97328.5
20	104364.4	104201.4	102040.9	101879.5	99746.2	99586.4	97480.5	97321.9
21	104362.6	104192.1	102040.1	101871.0	99746.2	99578.5	97480.9	97314.8
22	104360.2	104181.7	102038.3	101861.3	99745.2	99569.7	97480.7	97306.9
23	104356.6	104170.2	102035.5	101850.7	99743.0	99559.8	97479.2	97297.7
24	104351.8	104157.6	102031.4	101838.8	99739.7	99549.1	97476.9	97287.7
25	104345.7	104143.3	102026.2	101825.6	99735.2	99536.6	97473.1	97276.7
26	104337.4	104127.2	102018.6	101810.3	99728.9	99522.3	97467.5	97262.8
27	104326.5	104108.7	102008.9	101792.9	99719.9	99505.8	97460.0	97247.5
28	104313.3	104087.5	101996.4	101772.7	99708.4	99486.6	97448.9	97228.2
29	104296.8	104063.2	101981.0	101749.0	99693.9	99464.4	97435.6	97208.2
30	104281.1	104039.7	101966.3	101727.0	99680.2	99443.1	97421.8	97187.9

[a]Transition frequencies for $J_j \leq 27$ levels are generated from experimental term values reported by *Roncin et al.* [1998, 1999]. For $J_j = 28-30$, the calculated term values are used. The error in either case is less than 1 cm^{-1}.

non-uniform wavelength drifts are noticeable in Figure 4. However, the (0,2) band is a factor of ~10 weaker, making it necessary to carry out multiple scans over relatively long intervals. This in turn makes the measurement more susceptible to non-uniform wavelength drifts. The experimental spectrum shown in Figure 5 was obtained by summing ~100 scans over a period of ~146 h. Even though the non-uniform wavelength drift is not noticeable from scan to scan, the summation may introduce artifacts. The signal-to-noise ratio in Figure 5 is poorer than that in Figure 4 even taking account for a factor ~5 difference in signal. The spectral resolution in Figure 5 is also degraded from ~33 mÅ to ~36 mÅ. Furthermore, the shape of a weak transition sandwiched by two strong transitions may be distorted significantly by non-uniform drift.

[42] In Figure 4, excellent agreement is seen between the experimental high-resolution (~33 mÅ FWHM) and corresponding CSE-model spectra for the $c'_4\ ^1\Sigma_u^+(0) - X\ ^1\Sigma_g^+(1)$ band. Emissions from the $b'\ ^1\Sigma_u^+(1) - X\ ^1\Sigma_g^+(1)$ transition and other overlapping N_2 features have also been considered in the model. Except for the few J_j levels of the $b'\ ^1\Sigma_u^+(1)$ state in the region of the $b'\ ^1\Sigma_u^+(1) \sim c'_4\ ^1\Sigma_u^+(0)$ level crossing, the intensities of all other overlapping N_2 emission features are negligible. While the model does not include any contribution from atomic nitrogen emissions, it is apparent that the atomic nitrogen $2s2p^4\ ^2D - 2s^22p^3\ ^2D^o$ transitions, at 980.632 and 980.706 Å, are either absent or negligible.

[43] In Figure 5, which compares the experimental (solid line) high-resolution (~36 mÅ FWHM) and corresponding CSE-model (dotted line) spectra for the $c'_4\ ^1\Sigma_u^+(0) - X\ ^1\Sigma_g^+(2)$ band region, very good agreement is also found, except for the $P(9)$ and R-branch band head regions. In terms of integrated intensity, the $P(9)$ region in the observed spectrum is ~11% weaker than the model spectrum. However, the absence of the $P(9)$ peak and valley in the experimental spectrum, possibly due to the summing of multiple scans, makes the intensity difference more apparent. In the R-branch band head region, the model underestimates the intensity by as much as 50%. Since the model accurately reproduces the relative intensity of the R-branch band head region for the (0,1) band, the large difference in the (0,2) band head intensity is perhaps due to the approximate nature of the Boltzmann distribution (T = 150 K), obtained under a more stringent expansion condition. The model also reproduces the relative line intensities in the $c'_4\ ^1\Sigma_u^+(0) - X\ ^1\Sigma_g^+(2)$ and $b'\ ^1\Sigma_u^+(1) - X\ ^1\Sigma_g^+(2)$ bands very well, including the extremely weak features on the shorter wavelength side of 1002.5 Å, arising from the $b'\ ^1\Sigma_u^+(7) - X\ ^1\Sigma_g^+(4)$ transition. However, the intensities for the weak features on the longer wavelength side of 1003.63 Å, which primarily arise from the $c_3\ ^1\Pi_u(1) - X\ ^1\Sigma_g^+(3)$ transition, are overestimated by the model. This discrepancy might be removed by an improvement in the $c_3\ ^1\Pi_u - X\ ^1\Sigma_g^+$ diabatic electronic transition moment, but probably not without introducing other discrepancies elsewhere in the $c_3\ ^1\Pi_u -$

Table 6. Transition Frequencies of the $b'\ ^1\Sigma_u^+(1) - X\ ^1\Sigma_g^+(v_i)$ ($v_i = 0–3$) Bands (cm^{-1})[a]

	$b'\ ^1\Sigma_u^+(1) - X\ ^1\Sigma_g^+(0)$		$b'\ ^1\Sigma_u^+(1) - X\ ^1\Sigma_g^+(1)$		$b'\ ^1\Sigma_u^+(1) - X\ ^1\Sigma_g^+(2)$		$b'\ ^1\Sigma_u^+(1) - X\ ^1\Sigma_g^+(3)$	
J_j	$R(J_j-1)$	$P(J_j+1)$	$R(J_j-1)$	$P(J_j+1)$	$R(J_j-1)$	$P(J_j+1)$	$R(J_j-1)$	$P(J_j+1)$
0		104414.2		102084.3		99783.0		97510.6
1	104420.4	104408.4	102090.4	102078.6	99789.2	99777.5	97516.6	97505.1
2	104420.9	104401.0	102091.0	102071.4	99789.7	99770.4	97517.3	97497.9
3	104419.9	104392.1	102090.1	102062.6	99789.0	99761.6	97516.6	97489.4
4	104417.2	104381.4	102087.6	102052.1	99786.6	99751.3	97514.2	97479.3
5	104412.6	104368.8	102083.1	102039.7	99782.2	99739.1	97509.9	97467.3
6	104406.7	104355.0	102077.3	102026.1	99776.6	99725.8	97504.6	97454.2
7	104399.0	104339.3	102069.9	102010.8	99769.3	99710.7	97497.5	97439.4
8	104389.7	104322.0	102060.8	101993.8	99760.5	99694.0	97488.9	97423.0
9	104378.8	104303.2	102050.3	101975.3	99750.2	99676.0	97478.9	97405.3
10	104367.1	104283.6	102038.8	101955.9	99739.1	99657.1	97468.1	97386.8
11	104347.8	104256.4	102019.8	101929.2	99720.5	99630.7	97449.8	97360.9
12	104333.2	104234.2	102005.5	101907.1	99706.7	99609.0	97436.4	97339.6
13	104315.6	104208.1	101988.4	101882.1	99689.9	99584.5	97420.2	97315.6
14	104296.8	104181.0	101969.7	101855.4	99671.7	99558.4	97402.3	97290.0
15	104274.7	104151.7	101948.7	101826.5	99651.1	99530.1	97382.3	97262.3
16	104251.8	104120.7	101926.2	101796.3	99629.2	99500.3	97360.8	97233.3
17	104227.1	104088.2	101902.0	101764.2	99605.5	99468.9	97337.7	97202.4
18	104200.7	104054.1	101876.2	101730.5	99580.2	99435.9	97313.2	97170.1
19	104172.7	104017.8	101848.7	101695.3	99553.4	99401.3	97286.9	97136.0
20	104143.0	103980.0	101819.5	101658.1	99524.8	99365.0	97259.1	97100.5
21	104111.2	103940.6	101788.7	101619.6	99494.8	99327.0	97229.4	97063.3
22	104077.9	103899.5	101756.0	101579.1	99462.9	99287.4	97198.4	97024.6
23	104043.0	103856.7	101721.9	101537.2	99429.4	99246.2	97165.7	96984.1
24	104006.3	103812.2	101685.9	101493.4	99394.3	99203.6	97131.5	96942.3
25	103967.9	103765.6	101648.4	101447.9	99357.5	99158.9	97095.4	96899.0
26	103927.9	103717.6	101609.0	101400.8	99319.3	99112.7	97058.0	96853.2
27	103885.6	103667.8	101568.0	101351.9	99279.0	99064.9	97019.0	96806.6
28	103842.1	103616.3	101525.3	101301.5	99237.2	99015.5	96977.7	96757.0
29	103797.4	103563.8	101481.6	101249.6	99194.5	98965.0	96936.2	96708.8
30	103749.3	103507.9	101434.5	101195.2	99148.5	98911.3	96890.0	96656.1

[a]Transition frequencies are generated from experimental term values reported by *Roncin et al.* [1998, 1999]. The error in transition frequency is no more than several tenth of 1 cm^{-1}.

$X\ ^1\Sigma_g^+$ system (see comments above). Atomic nitrogen and the nitrogen ion are negligible emitters in the wavelength range of Figure 5 because no significant relative intensity variations were observed in a measurement with ~20 eV excitation energy, where the production of N (and thus N^+) is energetically impossible.

[44] As a consequence of the homogenous coupling between the $b'\ ^1\Sigma_u^+(1)$ and $c'_4\ ^1\Sigma_u^+(0)$ states, and crossing of the rotational term series, emission from some levels of the $b'\ ^1\Sigma_u^+(1)$ state, e.g., $J_j = 8–12$, overlap with those from the $c'_4\ ^1\Sigma_u^+(0)$ state. The *FUSE* observations, limited to $v_i \leq 9$, of the terrestrial thermosphere reported by *Bishop et al.* [2005, 2007] have shown prominent $c'_4\ ^1\Sigma_u^+(0)$ and $b'\ ^1\Sigma_u^+(1) - X\ ^1\Sigma_g^+(v_i \leq 9)$ emission. The difference in the v_i dependence of the Franck-Condon factors for the $b'\ ^1\Sigma_u^+(1) - X\ ^1\Sigma_g^+(v_i)$ and $c'_4\ ^1\Sigma_u^+(0) - X\ ^1\Sigma_g^+(v_i)$ transitions has a profound effect on their relative intensities in the emission spectrum. The Franck-Condon factor for the (diabatic) $b'\ ^1\Sigma_u^+(1) - X\ ^1\Sigma_g^+(0)$ transition is a factor of $\sim 2 \times 10^5$ smaller than its (diabatic) $c'_4\ ^1\Sigma_u^+(0) - X\ ^1\Sigma_g^+(0)$ counterpart. If the $b'\ ^1\Sigma_u^+(1) \sim c'_4\ ^1\Sigma_u^+(0)$ coupling were absent, the excitation cross section for the (diabatic) $b'\ ^1\Sigma_u^+(1) - X\ ^1\Sigma_g^+(0)$ transition would be negligible. Even with $b'\ ^1\Sigma_u^+(1) \sim c'_4\ ^1\Sigma_u^+(0)$ coupling, the excitation cross sections of the $b'\ ^1\Sigma_u^+(1)$ rotational levels, with the exception of $J_j = 8–12$, are about two orders of magnitude smaller than their $c'_4\ ^1\Sigma_u^+(0)$ counterparts (see Tables 3 and 4). Thus if the transition probabilities for the $c'_4\ ^1\Sigma_u^+(0) - X\ ^1\Sigma_g^+(v_i)$ transitions are larger than, or comparable to, those of the $b'\ ^1\Sigma_u^+(1) - X\ ^1\Sigma_g^+(v_i)$ transitions, the observed $c'_4\ ^1\Sigma_u^+(0) - X\ ^1\Sigma_g^+(v_i)$ intensity will be much stronger than that of the $b'\ ^1\Sigma_u^+(1) - X\ ^1\Sigma_g^+(v_i)$ transition. This is the case for the $v_i = 0$ to 4 levels. For $v_i > 4$, the rapid decrease of the Franck-Condon factor for the $c'_4\ ^1\Sigma_u^+(0) - X\ ^1\Sigma_g^+(v_i)$ transitions, and simultaneous rapid increase of that for the $b'\ ^1\Sigma_u^+(1) - X\ ^1\Sigma_g^+(v_i)$ transitions, make the transition probabilities for the former significantly smaller than those of the latter. In fact the $c'_4\ ^1\Sigma_u^+(0) - X\ ^1\Sigma_g^+(v_i > 4)$ transition probabilities are significant only because of $b'\ ^1\Sigma_u^+(1) \sim c'_4\ ^1\Sigma_u^+(0)$ coupling. The offsetting effects make the emission intensities of $c'_4\ ^1\Sigma_u^+(0) - X\ ^1\Sigma_g^+(v_i > 4)$ and $b'\ ^1\Sigma_u^+(1) - X\ ^1\Sigma_g^+(v_i > 4)$ approximately (within ±20%) equal.

[45] The $c'_4\ ^1\Sigma_u^+$ state also decays spontaneously to the $a\ ^1\Pi_g$ and $a''\ ^1\Sigma_g^+$ states. *Filippelli et al.* [1984] have estimated that the emission branching ratio to the $a\ ^1\Pi_g$ state is <0.6%. The branching ratio to $a''\ ^1\Sigma_g^+$, while unknown, must be very small because the transition frequency of the $c'_4\ ^1\Sigma_u^+(0) - X\ ^1\Sigma_g^+(0)$ band is more than 19 times of that of the $c'_4\ ^1\Sigma_u^+(0) - a''\ ^1\Sigma_g^+(0)$ band [*Cossart and Cossart-Magos*, 2004]. The radiative lifetimes of the $J_j = 0$ and 1 levels of the $c'_4\ ^1\Sigma_u^+(0)$ state, obtained from the calculated transition probabilities, are 840 ps, which are consistent with the 820 ± 50 ps estimated by *Liu et al.* [2005a] and the upper limit of 870 ps obtained by *Walter et al.* [1994]. In a coupled-channel picture, the diabatic $c'_4\ ^1\Sigma_u^+$ and $c_3\ ^1\Pi_u^e$ states, both members of the 3*p* Rydberg complex, have a strong rotational interac-

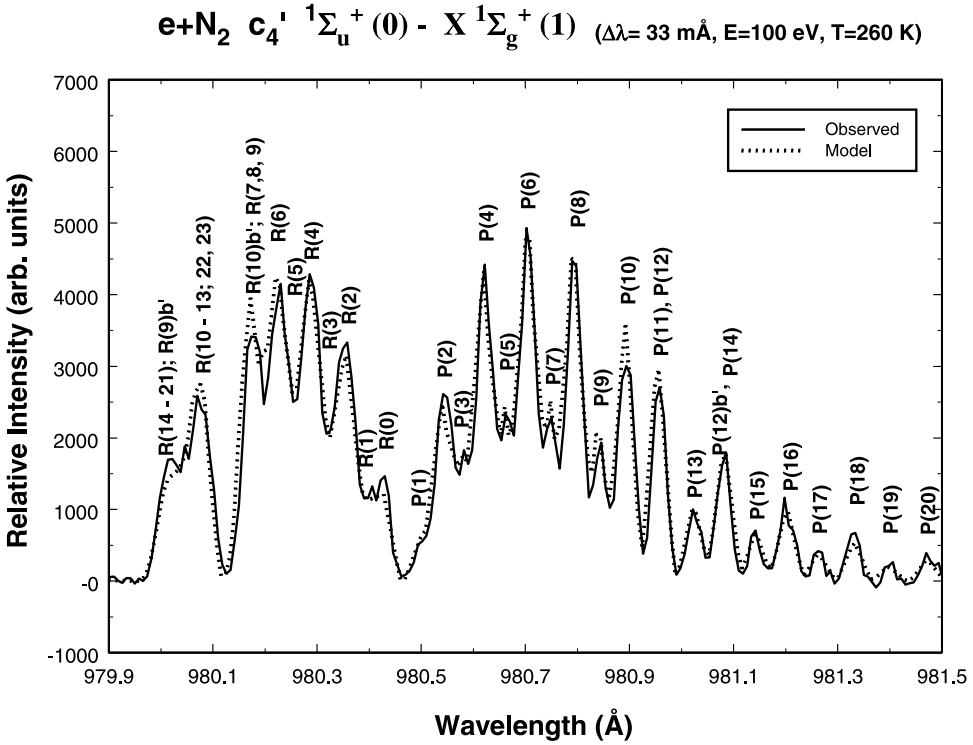

Figure 4. Comparison of high-resolution experimental (solid line) and CSE-model (dotted line) e + N_2 emission spectra for the $c'_4\ ^1\Sigma_u^+(0) - X\ ^1\Sigma_g^+(1)$ transition. The transition is labeled in standard notation $\Delta J(J_i)$ with appropriate upper electronic state designation. When the electronic designation is omitted, the transition is assumed to be from the $c'_4\ ^1\Sigma_u^+(0) - X\ ^1\Sigma_g^+(1)$ band. When electronic label is b', the transition is from the $b'\ ^1\Sigma_u^+(1) - X\ ^1\Sigma_g^+(1)$ band. The experimental spectrum was obtained under essentially the same conditions as those described by *Liu et al.* [2005a], except that the N_2 pressure was $(0.9 \pm 0.1) \times 10^{-4}$ Torr. The spectral resolution is ~33 mÅ FWHM. A factor of ~14 increase in N_2 pressure from that of *Liu et al.* [2005a] results in a decrease in rotational temperature from ~300 K to ~260 K. The overlapping $b'\ ^1\Sigma_u^+(7) - X\ ^1\Sigma_g^+(3)$ emission, which peaks near the *R*-branch band head at 980 Å, is much weaker that the $c'_4\ ^1\Sigma_u^+(0) - X\ ^1\Sigma_g^+(1)$ emission. Atomic nitrogen $2s2p^4\ ^2D - 2s^22p^3\ ^2D^o$ emission lines, at 980.632 and 980.706 Å, are either absent or negligible.

tion [*Lefebvre-Brion and Field*, 2004]. In the equivalent local-perturbation picture, the $b\ ^1\Pi_u^e(4)$, $b\ ^1\Pi_u^e(5)$ and $c_3\ ^1\Pi_u^e(0)$ levels are the primary rotational perturbers of the $c'_4\ ^1\Sigma_u^+(0)$ level [*Liu and Shemansky*, 2006]. The $^1\Sigma_u^+ \sim\ ^1\Pi_u^e$ coupling also provides the $c'_4\ ^1\Sigma_u^+(0)$ levels with a primary, J_j-dependent, predissociation mechanism by $^1\Pi_u(^e$ levels, which, in turn, are predissociated by the $C\ ^3\Pi_u$ and $C'\ ^3\Pi_u$ states via spin-orbit coupling [*Lewis et al.*, 2005a, 2005b; *Haverd et al.*, 2005]. The lifetime of the $J_j = 0$ level of the $c'_4\ ^1\Sigma_u^+(0)$ state, therefore, is the predissociation-free lifetime.

[46] High-resolution photoabsorption measurements by *Stark et al.* [1992, 2000, 2005] have shown, in many cases, large deviations of the *R*:*P*-branch oscillator-strength ratio from the corresponding Hönl-London factor ratio, and very strong *J*-dependence of some *Q*-branch oscillator strengths. The CSE calculation of *Haverd et al.* [2005] has achieved very good agreement with experimental *Q*-branch oscillator strengths for transitions to the $^1\Pi_u^f$ states. They attributed any strong *J*-dependence of the vibronic oscillator strength to the quantum interference caused by strong electrostatic coupling within the $^1\Pi_u$ manifold. In addition to the electrostatic coupling, the *P*- and *R*-branch transitions are affected by $^1\Sigma_u^+ \sim\ ^1\Pi_u^e$ coupling. *Liu and Shemansky* [2006], by considering the localized coupling among the $b'\ ^1\Sigma_u^+(1)$, $c'_4\ ^1\Sigma_u^+(0)$, $b\ ^1\Pi_u^e(4)$, $b\ ^1\Pi_u^e(5)$ and $c_3\ ^1\Pi_u^e(0)$ levels, have obtained accurate *P*- and *R*-branch oscillator strengths for transitions between these levels and the $X\ ^1\Sigma_g^+(0)$ level. Because of the strong *J*-dependence of the vibronic oscillator strength for the three $^1\Pi_u^e$ levels, it was necessary to use dipole matrix elements derived from the experimental *Q*-branch oscillator strengths for the $b\ ^1\Pi_u^f(4)$, $b\ ^1\Pi_u^f(5)$, and $c_3\ ^1\Pi_u^f(0) - X\ ^1\Sigma_g^+(0)$ bands. However, as the dipole matrix elements of the $b\ ^1\Pi_u^f(4)$, $b\ ^1\Pi_u^f(5)$, and $c_3\ ^1\Pi_u^f(0) - X\ ^1\Sigma_g^+(v_i > 0)$ transitions cannot be computed from their diabatic vibrational overlap integrals, the local-coupling model of *Liu and Shemansky* [2006] cannot be extended to the $v_i > 0$ levels of the $X\ ^1\Sigma_g^+$ state. In this regard, the more sophisticated CSE model employed here provides a more accurate and versatile representation of the experimental results.

[47] The present experimental investigation has not addressed the predissociation rate of the $c'_4\ ^1\Sigma_u^+(0)$ level, which is another important quantity for atmospheric modeling. Even though the $c'_4\ ^1\Sigma_u^+(0)$ level is known to be predissociated by $^1\Sigma_u^+ \sim\ ^1\Pi_u^e$ coupling, no systematic measurements on individual rotational levels have been carried out, although *Ubachs et al.* [2001] have detected

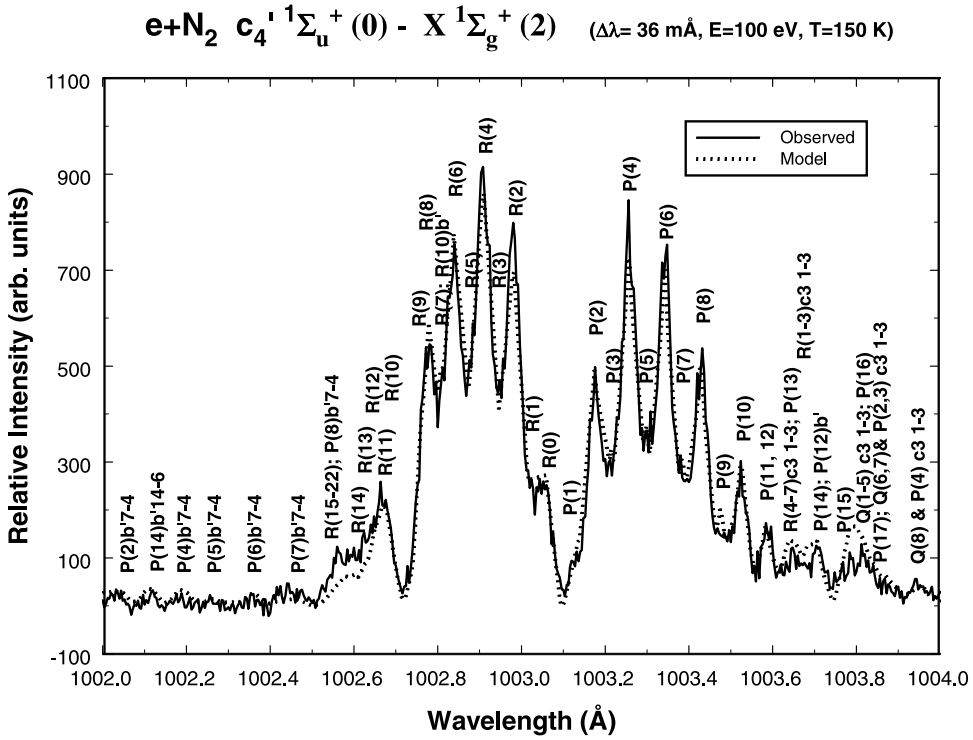

Figure 5. Comparison of high-resolution experimental (solid line) and CSE-model (dotted line) e + N_2 emission spectra for the $c'_4\ ^1\Sigma_u^+(0) - X\ ^1\Sigma_g^+(2)$ transition. The transitions are labeled in terms of $\Delta J(J_i)\beta\ v_j - v_i$, where β represents the upper electronic state. When the vibronic label, $\beta v_j - v_i$, is omitted, the transition is from the $c'_4\ ^1\Sigma_u^+(0) - X\ ^1\Sigma_g^+(2)$ band. When only β (i.e., no $v_j - v_i$) is specified, the transition belongs to the $b'\ ^1\Sigma_u^+(1) - X\ ^1\Sigma_g^+(2)$ band. The experimental conditions are similar to those of Figure 4, except that the N_2 pressure was $\sim 3.3 \times 10^{-4}$ Torr and a much longer integration time was employed to compensate for the weaker signal. A factor of $\sim$3 increase in N_2 pressure from that of Figure 4 results in a decrease in rotational temperature to $\sim$150 K. The very weak $b'\ ^1\Sigma_u^+(7) - X\ ^1\Sigma_g^+(4)$ emission, between 1001.9 and 1002.5 Å, is also well reproduced by the model. However, intensities for the peaks at longer wavelengths than 1003.63 Å, primarily from the $c_3\ ^1\Pi_u(1) - X\ ^1\Sigma_g^+(3)$ band, are somewhat overestimated in the model. See section 4 for discussion of the discrepancy.

some J-dependence in the lifetime by using pump-probe laser techniques without rotational resolution. While *Liu et al.* [2005a] provided a crude estimate of the $c'_4\ ^1\Sigma_u^+(0)$ predissociation yields, their results were based on interpolation and extrapolation of the experimental lifetimes of *Ubachs et al.* [2001] and application of the $c'_4\ ^1\Sigma_u^+(0) - X\ ^1\Sigma_g^+(0)$ Franck-Condon factor of *Whang et al.* [1996], both of which can lead to significant errors. In principle, the predissociation yield of a (v_j, J_j) level can be obtained as the fraction of the total emission cross section from the level to the excitation cross section to the level. The excitation cross section of the $c'_4\ ^1\Sigma_u^+(0)$ state can be obtained from the excitation function measured by *Ajello et al.* [1989] and the photoabsorption oscillator strength measured by *Stark et al.* [2000, 2005], or calculated by the CSE method in the present study. It can also be obtained directly from electron energy loss work of *Khakoo et al.* [2007]. If the absolute emission cross section of the $c'_4\ ^1\Sigma_u^+(v_j, J_j)$ level to the $X\ ^1\Sigma_g^+(0)$ level, or an $X\ ^1\Sigma_g^+(v_j > 0)$ level, can be measured accurately, the transition probabilities calculated in the present study enable a reliable evaluation of the total emission cross section. In this way, both predissociation yield and total transition probability, $A(v_j, J_j)$, can be determined. Work is in progress to measure the absolute emission cross section of the $c'_4\ ^1\Sigma_u^+(0) - X\ ^1\Sigma_g^+(0)$ band under high-resolution and optically thin conditions. After the measurements are completed, a forthcoming article will present excitation cross sections and compare the measured and CSE calculated predissociation yields and emission cross sections of the $c'_4\ ^1\Sigma_u^+(v_j = 0, J_j)$ levels.

[48] In summary, relative emission intensities for the $c'_4\ ^1\Sigma_u^+(0) - X\ ^1\Sigma_g^+(1\text{-}3)$ bands of N_2 have been determined accurately, using low-resolution electron-impact-induced emission spectroscopy. A CSE-model analysis of the experimental relative intensities and photoabsorption oscillator strengths [*Stark et al.*, 2000, 2005] has allowed the determination of the diabatic $c'_4\ ^1\Sigma_u^+ - X\ ^1\Sigma_g^+$ electronic transition moment and calculation of the $c'_4\ ^1\Sigma_u^+(0) - X\ ^1\Sigma_g^+(v_i)$ and $b'\ ^1\Sigma_u^+(1) - X\ ^1\Sigma_g^+(v_i)$ line transition probabilities. The accuracy of the calculated transition probabilities has been further verified by comparison with high-resolution experimental emission spectra.

[49] **Acknowledgments.** This work has been partially supported by NSF ATM-0131210 and the Cassini UVIS contract with the University of Colorado. It has also partially been supported by the National Aeronautics and Space Administration (NASA) under grant no. NNG06GH76G issued

to SET through the Planetary Atmospheres Program, to the JPL through the Outer Planets Research Program, and to Wellesley College through grant NNG05GA03G. The experimental part of the research was performed at JPL, California Institute of Technology, under a contract with NASA. This work has also been partially supported by Australian Research Council Discovery Program grant no. DP0558962, and Part of the research was performed while CPM held a NASA Postdoctoral Fellowship at JPL.

[50] Wolfgang Baumjohann thanks Alexander Dalgarno and another reviewer for their assistance in evaluating this paper.

References

Abgrall, H., and E. Roueff (2003, private communication), Adiabatic transition probabilities the $B''B$, $^1\Sigma_u^+$ and D', $^1\Pi_u$–X, $^1\Sigma_g^+$ band systems of molecular hydrogen, unpublished.

Abgrall, H., and E. Roueff (2006), Theoretical calculations of excited rovibrational levels of HD. Term values and transition probabilities of VUV electronic bands, *Astron. Astrophys.*, *445*, 361–372, doi:10.1051/0004-6361:20053694.

Abgrall, H., E. Roueff, X. Liu, and D. E. Shemansky (1997), The emission continuum of electron-excited molecular hydrogen, *Astrophys. J.*, *481*, 557–566, doi:10.1086/304017.

Ajello, J. M., G. K. James, B. O. Franklin, and D. E. Shemansky (1989), Medium-resolution studies of extreme ultraviolet emission from N_2 by electron impact: Vibrational perturbations and cross sections of the $c'_4\ ^1\Sigma_u^+$ and $b'\ ^1\Sigma_u^+$ states, *Phys. Rev. A*, *40*, 3524–3555, doi:10.1103/PhysRevA.40.3524.

Ajello, J. M., G. K. James, and M. Ciocca (1998), High resolution EUV emission spectroscopy of the N_2 $c'\ ^1\Sigma_u^+$ $v' = 3$ and 4 levels by electron impact, *J. Phys. B*, *31*, 2437–2448, doi:10.1088/0953-4075/31/10/028.

Bishop, J., M. H. Stevens, and P. D. Feldman (2005), Molecular nitrogen Carroll-Yoshino $c'_4\ ^1\Sigma_u^+$ ($v' = 0$, $v'' > 2$) fluorescence in the thermospheric dayglow as seen by the Far Ultraviolet Spectroscopic Explorer, *AGU 2005 Spring Meeting*, abstract #SA41A-12, 2005.

Bishop, J., M. H. Stevens, and P. D. Feldman (2007), Molecular nitrogen Carroll-Yoshino $c'_4\ ^1\Sigma_u^+$ $v' = 0$ emission in the thermospheric dayglow as seen by the Far Ultraviolet Spectroscopic Explorer, *J. Geophys. Res.*, *112*, A10312, doi:10.1029/2007JA012389.

Broadfoot, A. K., et al. (1989), Ultraviolet spectrometer observations of Neptune and Triton, *Science*, *246*, 1459–1466, doi:10.1126/science.246.4936.1459.

Carroll, P. K., and C. P. Collins (1969), High resolution absorption studies of the $b\ ^1\Pi_u$ from $X\ ^1\Sigma_g^+$ system of nitrogen, *Can. J. Phys.*, *47*, 563–590.

Carroll, P. K., and K. Yoshino (1972), The $c_n\ ^1\Pi_u$ and $c'_n\ ^1\Sigma_u^+$ Rydberg states of N_2: High resolution studies, *J. Phys. B*, *5*, 1614–1635, doi:10.1088/0022-3700/5/8/025.

Carroll, P. K., C. P. Collins, and K. Yoshino (1970), The high energy $^1\Sigma_u^+$ states of N_2, *J. Phys. B.*, *3*, L127–L131, doi:10.1088/0022-3700/3/11/018.

Carter, V. L. (1972), High-resolution N2 absorption study from 730 to 980 Å, *J. Chem. Phys.*, *56*, 4195–4205, doi:10.1063/1.1677835.

Chan, W. F., G. Cooper, R. N. S. Sodhi, and C. E. Brion (1993), Absolute optical oscillator strengths for discrete and continuum photoabsorption of molecular nitrogen (11–200 eV), *Chem. Phys.*, *170*, 81–97, doi:10.1016/0301-0104(93)80095-Q.

Cochran, A. L., W. D. Cochran, and E. S. Barker (2000), N_2^+ and CO^+ in Comets 122P/1995 S1 (deVico) and C/1995 O1 (Hale-Bopp), *Icarus*, *146*, 583–593, doi:10.1006/icar.2000.6413.

Cossart, D., and C. Cossart-Magos (2004), New Rydberg-Rydberg transitions in N_2. Identification of the $d_3\ ^1\Sigma_g^+$ state, *J. Chem. Phys.*, *121*, 7148–7152, doi:10.1063/1.1791154.

Edwards, S. A., W.-U. L. Tchang-Brillet, J.-Y. Roncin, F. Launay, and F. Rostas (1995), Modelling the VUV emission spectrum of N_2: Preliminary results on the effects of rotational interactions on line intensities, *Planet. Space Sci.*, *43*, 67–73, doi:10.1016/0032-0633(94)00088-9.

Feldman, P. D., D. J. Sahnow, J. W. Kruk, E. M. Murphy, and H. W. Moos (2001), High-resolution FUV spectroscopy of terrestrial day airglow with the Far Ultraviolet Spectroscopic Explorer, *J. Geophys. Res.*, *106*, 8119–8129.

Filippelli, A. R., S. Chung, and C. C. Lin (1984), Electron-impact excitation of the $D\ ^3\Sigma_u^+$ and $c'_4\ ^1\Sigma_u^+$ Rydberg states of N_2, *Phys. Rev. A.*, *29*, 1709–1728, doi:10.1103/PhysRevA.29.1709.

Geiger, J., and B. Schröder (1969), Intensity perturbations due to configuration interaction observed in the electron energy-loss spectrum of N_2, *J. Chem. Phys.*, *50*, 7–11, doi:10.1063/1.1670870.

Gürtler, P., V. Saile, and E. E. Koch (1977), High resolution absorption spectrum of nitrogen in the vacuum ultraviolet, *Chem. Phys. Lett.*, *48*, 245–250, doi:10.1016/0009-2614(77)80308-4.

Hall, D. T., D. E. Shemansky, and T. Tripp (1992), A reanalysis of Voyager UVS observations of Titan, ESA Symposium on Titan (N92-32348 23-91), 67–74.

Haverd, V. E., B. R. Lewis, S. T. Gibson, and G. Stark (2005), Rotational effects in the band oscillator strengths and predissociation linewidths for the lowest $^1\Pi_u - X\ ^1\Sigma_g^+$ transitions of N_2, *J. Chem. Phys.*, *123*, 214304, doi:10.1063/1.2134704.

Helm, H., and P. C. Cosby (1989), Product branching in predissociation of the $c_4\ ^1\Pi_u$, $c'_5\ ^1\Sigma_u^+$, and $b'\ ^1\Sigma_u^+$ states of N_2, *J. Chem. Phys.*, *90*, 4208–4215, doi:10.1063/1.455777.

Helm, H., I. Hazell, and N. Bjerre (1993), Lifetimes and Ryberg-valence state mixing of the $c'_4\ ^1\Sigma_u^+$ ($v = 4$) and $c_3\ ^1\Pi_u$ ($v = 4$) states of N_2, *Phys. Rev. A*, *48*, 2762–2771, doi: 10.1103/PhysRevA.48.2762.

Iro, N., D. Gautier, F. Hersant, D. Bockelee-Morvan, and J. I. Lunine (2003), An interpretation of the nitrogen deficiency in comets, *Icarus*, *161*, 511–532, doi:10.1016/S0019-1035(02)00038-6.

James, G. K., J. M. Ajello, B. Franklin, and D. E. Shemansky (1990), Medium resolution studies of extreme ultraviolet emission from N_2 by electron impact: The effect of predissociation on the emission cross section of the $b\ ^1\Pi_u$ state, *J. Phys. B.*, *23*, 2055–2081, doi:10.1088/0953-4075/23/12/015.

Jonin, C., X. Liu, J. M. Ajello, G. K. James, and H. Abgrall (2000), High-Resolution Electron-Impact Emission Spectrum of H2. I. Cross Sections and Emission Yields 900-1200 Å, *Astrophys. J. Suppl. Ser.*, *129*, 247–266, doi:10.1086/313414.

Kam, A. W., J. R. Lawall, M. D. Lindsay, F. M. Pipkin, R. C. Short, and P. Zhao (1989), Precise spectroscopy and lifetime measurement of electron-impact-excited N_2: The $c'_4\ ^1\Sigma_u^+$ ($v = 3$) Rydberg level, *Phys. Rev. A*, *40*, 1279–1288, doi:10.1103/PhysRevA.40.1279.

Kawamoto, Y., M. Fujitake, and N. Ohashi (1997), Near-infrared diode laser spectroscopy of the nitrogen molecule in Rydberg State: Analysis of the $c_3\ ^1\Pi_u - a''\ ^1\Sigma_g^+$,v = 1-0 band, *J. Mol. Spectrosc.*, *185*, 330–335, doi:10.1006/jmsp.1997.7404.

Khakoo, M. A., S. Wang, P. V. Johnson, C. P. Malone, and I. Kanik (2007), *Phys. Rev. A*, in preparation.

Knauth, D. C., B.-G. Anderson, S. R. McCandliss, and H. W. Moos (2004), The interstellar N_2 abundance towards HD 124314 from far-ultraviolet observations, *Nature*, *429*, 636–638, doi:10.1038/nature02614.

Lawrence, G. M., D. L. Mickey, and K. Dressler (1968), Absolute oscillator strengths of the strongest bands within the dipole-allowed absorption spectrum of nitrogen, *J. Chem. Phys.*, *48*, 1989–1994, doi:10.1063/1.1669002.

Lefebvre-Brion, H., and R. W. Field (2004), *The Spectra and Dynamics of Diatomic Molecules*, pp. 144, 386-403, Academic Press, Amsterdam.

Levelt, P., and W. Ubachs (1992), XUV-laser spectroscopy of the $c'_4\ ^1\Sigma_u^+$, v = 0 and $c_3\ ^1\Pi_u$, v = 0 Rydberg states of N_2, *Chem. Phys.*, *163*, 263–275, doi:10.1016/0301-0104(92)87107-K.

Lewis, B. R., S. T. Gibson, W. Zhang, H. Lefebvre-Brion, and J. M. Robbe (2005a), Predissociation mechanism for the lowest $^1\Pi_u$ states of N_2, *J. Chem. Phys.*, *122*, 144,302–144,310, doi:10.1063/1.2137722.

Lewis, B. R., S. T. Gibson, J. P. Sprengers, W. Ubachs, A. Johnsson, and C.-G. Wahlstrom (2005b), Lifetime and predissociation yield of $^{14}N_2$ $b\ ^1\Pi_u$ (v = 1) revisited: Effects of rotation, *J. Chem. Phys.*, *123*, 236,101–236,103, doi:10.1063/1.2137722.

Lewis, B. R., A. N. Heays, S. T. Gibson, H. Lefebvre-Brion, and R. Lefebvre (2007), *J. Chem. Phys.*, manuscript in preparation.

Liu, X., and D. E. Shemansky (2006), A simple model for N_2 line oscillator strengths of the $b'\ ^1\Sigma_u^+(1)$, $c'_4\ ^1\Sigma_u^+(0)$, $b\ ^1\Pi_u^e(4)$, $b\ ^1\Pi_u^e(5)$ and $c_3\ ^1\Pi_u^e(0) - X\ ^1\Sigma_g^+(0)$ bands, *Astrophys. J.*, *645*, 1560–1566, doi:10.1086/504465.

Liu, X., S. M. Ahmed, R. A. Multari, G. K. James, and J. M. Ajello (1995), High-resolution electron-impact study of the far-ultraviolet emission spectrum of molecular hydrogen, *Astrophys. J. Suppl. Ser.*, *101*, 375–399, doi:10.1086/192246.

Liu, X., D. E. Shemansky, H. Abgrall, E. Roueff, D. Dziczek, D. L. Hansen, and J. M. Ajello (2002), Time-resolved electron impact study of excitation of H2 singlet-gerade states from cascade emission in the vacuum ultraviolet region, *Astrophys. J. Suppl. Ser.*, *138*, 229–245, doi:10.1086/323630.

Liu, X., D. E. Shemansky, H. Abgrall, E. Roueff, S. M. Ahmed, and J. M. Ajello (2003), Electron impact excitation of H2: Resonance excitation of $B\ ^1\Sigma_u^+$ ($J_j = 2$, $v_j = 0$) and effective excitation function of EF $^1\Sigma_g^+$, *J. Phys. B.*, *36*, 173–196, doi:10.1088/0953-4075/36/2/30.

Liu, X., D. E. Shemansky, M. Ciocca, I. Kanik, and J. M. Ajello (2005a), Analysis of the physical properties of the N_2 $c'_4\ ^1\Sigma_u^+$ (0) – $X\ ^1\Sigma_g^+$ (0) transition, *Astrophys. J.*, *623*, 579–584, doi:10.1086/428641.

Liu, X., D. E. Shemansky, and J. T. Hallett (2005b), The high altitude sunlit Titan ionosphere, *AGU, 2005 Fall Meeting*, abstract #P33C-0262.

Maret, S., E. A. Bergin, and J. Lada (2006), A low fraction of nitrogen in molecular form in a dark cloud, *Nature*, *442*, 425–427, doi:10.1038/nature04919.

Meier, R. R. (1991), Ultraviolet spectroscopy and remote sensing of the upper atmosphere, *Space Sci. Rev.*, *58*, 1–186, doi:10.1007/BF01206000.

Morrison, M. D., C. W. Bowers, P. D. Feldman, and R. R. Meier (1990), The EUV dayglow at high spectral resolution, *J. Geophys. Res.*, *95*, 4113–4127.

Oertel, H., M. Kratzat, J. Imschweiler, and T. Noll (1981), Fluorescence from $^1\Pi_u$ and $^1\Sigma^+_u$ states of molecular nitrogen excited with synchrotron radiation between 12.4 and 18.8 eV, *Chem. Phys. Lett.*, *82*, 552–556, doi:10.1016/0009-2614 (81)85439-5.

Romick, G. J., J.-H. Yee, M. F. Morgan, D. Morrison, L. J. Paxton, and C.-I. Meng (1999), Polar cap optical observations of topside (>900 km) molecular nitrogen ions, *Geophys. Res. Lett.*, *26*, 1003–1006, doi:10.1029/1999GL900091.

Roncin, J.-Y., J.-L. Subtil, and F. Launay (1998), The high-resolution vacuum ultraviolet emission spectrum of molecular nitrogen from 82.6 to 124.2 nm: Level energies of 10 excited singlet electronic states, *J. Mol. Spectrosc.*, *188*, 128–137, doi:10.1006/jmsp.1997.7497.

Roncin, J.-Y., F. Launay, H. Bredohl, and I. Dubois (1999), The vacuum ultraviolet absorption bands of the pink afterglow spectrum of molecular nitrogen revisited at high resolution, *J. Mol. Spectrosc.*, *194*, 243–249, doi:10.1006/jmsp.1998.7773.

Shemansky, D. E., J. M. Ajello, and D. T. Hall (1985), Electron impact excitation of H_2: Rydberg band systems and benchmark dissociative cross section for H Lyman alpha, *Astrophys. J.*, *296*, 765–773, doi:10.1086/163493.

Shemansky, D. E., I. Kanik, and J. M. Ajello (1995), Fine-Structure Branching in N_2 $c'_4\ ^1\Sigma_u^+(0)$, *Astrophys. J.*, *452*, 480–485, doi:10.1086/176320.

Smith, P. L., C. Heise, J. R. Esmond, and R. L. Kurucz (2001), 1995 Atomic Line Data by R. L. Kurucz and B. Bell, *Kurucz CD-ROM No. 23*, http://cfa-www.harvard.edu/amp/ampdata/kurucz23/sekur.html, Smithsonian Astrophysical Observatory, Cambridge, Mass.

Spelsberg, D., and W. Meyer (2001), Dipole-allowed excited states of N_2: Potential energy curves, vibrational analysis, and absorption intensities, *J. Chem. Phys.*, *115*, 6438–6449, doi:10.1063/1.1400139.

Sprengers, J. P., and W. Ubachs (2006), Lifetime and transition frequencies of several singlet ungerade states in N_2 between 106,000 and 109,000 cm^{-1}, *J. Mol. Spectrosc.*, *234*, 176–180, doi:10.1016/j.jms.2005.11.001.

Sprengers, J. P., W. Ubachs, K. G. H. Baldwin, B. R. Lewis, and W.-U. L. Tchang-Brillet (2003), Extreme ultraviolet laser excitation of isotopic molecular nitrogen: The dipole-allowed spectrum of $^{15}N_2$ and $^{14}N^{15}N$, *J. Chem. Phys.*, *119*, 3160–3173, doi:10.1063/1.1589478.

Sprengers, J. P., W. Ubachs, A. Johansson, A. L'Huillier, C.-G. Wahlstrom, R. Lang, B. R. Lewis, and S. T. Gibson (2004a), Lifetime and predissociation yield of $^{14}N_2$ $b\ ^1\Pi_u(v = 1)$, *J. Chem. Phys.*, *120*, 8973–8978, doi:10.1063/1.1704640.

Sprenger, J. P., A. Johansson, A. L'Huillier, C.-G. Wahlstrom, B. R. Lewis, and W. Ubachs (2004b), Pump-probe lifetime measurements on signlet *ungerade* states in molecular nitrogen, *Chem. Phys. Lett.*, *389*, 348, doi:10.1016/j.cplett.2004.03.116.

Sprengers, J. P., W. Ubachs, and K. G. H. Baldwin (2005), Isotopic variation of experimental lifetimes for the lowest $^1\Pi_u$ states of N_2, *Chem. Phys.*, *122*, 144,301–144,306, doi:10.1063/1.1869985.

Stahel, D., M. Leoni, and K. Dressler (1983), Nonadiabatic representations of the $^1O_u^+$ and $^1\Sigma_u$ states of the N_2 molecule, *J. Chem. Phys.*, *79*, 2541–2558, doi:10.1063/1.446166.

Stark, G., P.-L. Smith, K. P. Hubber, K. Yoshino, M. H. Stevens, and K. Ito (1992), Absorption band oscillator strength of N_2 transitions between 95.8 and 99.4 nm, *J. Chem. Phys.*, *97*, 4809–4814, doi:10.1063/1.463835.

Stark, G., K. P. Hubber, K. Yoshino, M.-C. Chan, T. Matusi, P. L. Smith, and K. Ito (2000), Line oscillator strength measurements in the 0-0 band of the $c'_4\ ^1\Sigma_u^+ \leftarrow X\ ^1\Sigma_g^+$ transition of N_2, *Astrophys. J.*, *531*, 321–328, doi:10.1086/308464.

Stark, G., K. P. Hubber, K. Yoshino, P.-L. Smith, and K. Ito (2005), Oscillator strength and linewidth measurements of dipole-allowed transitions in $^{14}N_2$ between 93.5 and 99.5 nm, *J. Chem. Phys.*, *123*, 214303-11, doi:10.1063/1.2134703.

Stark, G., A. N. Heays, B. R. Lewis, K. P. Huber, K. Yoshino, P. L. Smith, and K. Ito (2008), manuscript in preparation.

Stevens, M. H., R. R. Meier, R. R. Conway, and D. F. Strobel (1994), A resolution of the N_2 Carroll-Yoshino ($c'_4 - X$) band problem in the Earth's atmosphere, *J. Geophys. Res.*, *99*, 417–434.

Strickland, D. J., R. R. Meier, R. L. Walterscheid, J. D. Craven, A. B. Christensen, L. J. Paxton, D. Morrison, and G. Crowley (2004a), Quiet-time seasonal behavior of the thermosphere seen in the far ultraviolet dayglow, *J. Geophys. Res.*, *109*, A01302, doi:10.1029/2003JA010220.

Strickland, D. J., J. L. Lean, R. R. Meier, A. B. Christensen, L. J. Paxton, D. Morrison, J. D. Craven, R. L. Walterscheid, J. D. Judge, and D. R. McMullin (2004b), Solar EUV irradiance variability derived from terrestrial far ultraviolet dayglow observations, *Geophys. Res. Lett.*, *31*, L03801, doi:10.1029/2003GL018415.

Strobel, D. L., and D. E. Shemansky (1982), EUV emission from Titan's upper atmosphere – Voyager 1 encounter, *J. Geophys. Res.*, *87*, 1361–1368.

Trajmar, S., D. F. Register, and A. Chutjian (1983), Electron scattering by molecules II. Experimental methods and data, *Phys. Rep.*, *97*, 219–356.

Ubachs, W. (1997), Predissociative decay of the $c'_4\ ^1\Sigma_u^+$, v=0 state of N_2, *Chem. Phys. Lett.*, *268*, 201–206, doi:10.1016/S0009-2614(97)00179-6.

Ubachs, W., L. Tashiro, and R. N. Zare (1989), Study of the N_2 b, $^1\Pi_u$ state via 1+1 multiphoton ionization, *Chem. Phys.*, *130*, 1–13, doi:10.1016/0301-0104(89)87031-4.

Ubachs, W., I. Velchev, and A. de Lange (2000), Predissociation in $b\ ^1\Pi_u$, v(v = 1,4,5,6) levels of N_2, *J. Chem. Phys.*, *112*, 5711–5716, doi:10.1063/1.481145.

Ubachs, W., R. Lang, I. Velchev, W.-U. L. Tchang-Brillet, A. Johnsson, Z. S. Li, V. Lokhngyin, and C.-G. Wahlstrom (2001), Lifetime measurements on the $c'_4\ ^1\Sigma_u^+$, v = 0, 1 and 2 states of molecular nitrogen, *Chem. Phys.*, *270*, 215–225, doi:10.1016/S0301-0104(01)00378-0.

van Dishoeck, E. F., M. C. van Hemert, A. C. Allison, and A. Dalgarno (1984), Resonances in the photodissociation of OH by absorption into coupled $^2\Pi$ states: Adiabatic and diabatic formulations, *J. Chem. Phys.*, *81*, 5709–5724, doi:10.1063/1.447622.

Verma, R. D., and S. S. Jois (1984), Absorption spectrum of the $b'\ ^1\Sigma_u^+$ from $X\ ^1\Sigma_g^+$ transition of the N_2 molecule excited by the flash discharge technique, *J. Phys. B*, *17*, 3229–3237, doi:10.1088/0022-3700/17/16/006.

Walter, C. W., P. C. Cosby, and H. Helm (1993), $N(^4S^0)$, $N(^2D^0)$, and $N(^2P^0)$ yields in predissociation of excited singlet states of N_2, *J. Chem. Phys.*, *99*, 3553–3561, doi:10.1063/1.466152.

Walter, C. W., P. C. Cosby, and H. Helm (1994), Predissociation quantum yields of singlet nitrogen, *Phys. Rev.*, *50*, 2930–2936, doi:10.1103/PhysRevA.50.2930.

Walter, C. W., P. C. Cosby, and H. Helm (2000), Photoexcitation and predissociation intensities of the $c'_4\ ^1\Sigma_u^+$ (v=3 and 4), $c_3\ \{^1\Pi_u\}$ (v=3 and 4), and $b'\ ^1\Sigma_u^+$ (v=10, 12, 13, and 15) states of N_2, *J. Chem. Phys.*, *112*, 4621–4633, doi:10.1063/1.481090.

Watanabe, K., and F. F. Marmo (1956), Photoionization and total absorption cross section of gases. II. O_2 and N_2 in the region 850-1500 Å, *J. Chem. Phys.*, *25*, 965–971, doi:10.1063/1.1743151.

Whang, T.-J., G. Zhao, W. C. Stwalley, and C. Y. R. Wu (1996), Franck-Condon factors of the $b'\ ^1\Sigma_u^+ - X\ ^1\Sigma_g^+$, $c_3\ ^1\Pi_u - X\ ^1\Sigma_g^+$, $c'_4\ ^1\Sigma_u^+ - X\ ^1\Sigma_g^+$, $c'_4\ ^1\Sigma_u^+ - a\ ^1\Pi_g$ and $o_3\ ^1\Pi_u - X\ ^1\Sigma_g^+$ transition of N_2, *J. Quant. Spectrosc. Radiat. Transfer*, *55*, 335–344, doi:10.1016/0022-4073 (95)00169-7.

Wu, C. Y. R., H.-S. Fung, T. S. Singh, X.-L. Mu, J. B. Nee, S.-Y. Chiag, and D.-L. Judge (2007), Fluorescence excitation function produced through photoexcitation of the $b\ ^1\Pi_u$, $b'\ ^1\Sigma_u^+$, and the $c'_n\ ^1\Sigma_u^+$ states of N_2 in the 80–100 nm region, *J. Chem. Phys.*, *127*, 084314, doi:10.1063/1.2768923.

Yoshino, K., and Y. Tanaka (1977), High-resolution vuv absorption spectrum of N_2, homogeneous perturbation between $c'_4(0)\ ^1\Sigma_u^+$ and $b'(1)\ ^1\Sigma_u^+$ levels, *J. Mol. Spectrosc.*, *66*, 219–232, doi:10.1016/0022-2852(77)90212-0.

Yoshino, K., Y. Tanaka, P. K. Carroll, and P. Mitchell (1975), High resolution absorption spectrum of N2 in the vacuum-uv region, $o_{3,4}\ ^1\Pi_u - X\ ^1\Sigma_g^+$ bands, *J. Mol. Spectrosc.*, *54*, 87–109, doi:10.1016/0022-2852(75)90011-9.

Yoshino, K., D. E. Freeman, and Y. Tanaka (1979), High-resolution VUV absorption spectrum of N_2 $c'_4\ ^1\Sigma_u^+ \leftarrow X\ ^1\Sigma_g^+$ bands, *J. Mol. Spectrosc.*, *76*, 153–163, doi:10.1016/0022-2852(79)90224-8.

Zipf, E. C., and R. W. McLaughlin (1978), On the dissociation of nitrogen by electron impact and by E.U.V. photo-absorption, *Planet. Space Sci.*, *26*, 449–462, doi:10.1016/0032-0633(78)90066-1.

J. M. Ajello, P. V. Johnson, I. Kanik, and C. P. Malone, Jet Propulsion Laboratory, California Institute of Technology, 4800 Oak Grove Drive, Pasadena, CA 91109, USA. (paul.v.johnson@jpl.nasa.gov; charles.malone@jpl.nasa.gov)

S. T. Gibson, A. N. Heays, and B. R. Lewis, Research School of Physical Sciences and Engineering, The Australian National University, Canberra, Australian Capital Territory 0200, Australia. (alan.heays@anu.edu.au; brenton.lewis@anu.edu.au)

X. Liu and D. E. Shemansky, Planetary and Space Science Division, Space Environment Technologies, 320 N. Halstead, Pasadena, CA 91107, USA. (xliu@spacenvironment.net; dshemansky@spacenvironment.net)

G. Stark, Department of Physics, Wellesley College, Wellesley, MA 02481, USA. (gstark@wellesley.edu)